Atomic layer deposited Er_2O_3 for signal amplification in silicon based waveguides

Lasse Pakarinen

School of Electrical Engineering

Thesis submitted for examination for the degree of Master of Science in Technology.

Espoo 01.06.2017

Thesis supervisor:

Prof. Zhipei Sun

Thesis advisor:

M.Sc. Anton Autere

Aalto University
School of Electrical
Engineering

AALTO UNIVERSITY
SCHOOL OF ELECTRICAL ENGINEERING

ABSTRACT OF THE
MASTER'S THESIS

Author: Lasse Pakarinen

Title: Atomic layer deposited Er_2O_3 for signal amplification in silicon based waveguides

Date: 01.06.2017 Language: English Number of pages: 8+54

Department of Electronics and Nanoengineering

Professorship: Micro- and Nanosciences

Supervisor: Prof. Zhipei Sun

Advisor: M.Sc. Anton Autere

Silicon photonics has been utilized in a range of applications, from sensing to all optical signal processing. However, it is challenging to realize active components like amplifiers and lasing with silicon, mainly due to its indirect bandgap. The unique physical properties of erbium as a gain material are well known, especially for fiber optics. Atomic layer deposition is an excellent technology for accurate and conformal thin-film deposition on various surface geometries. Combining the properties of silicon photonics, erbium, and atomic layer deposition can potentially create new opportunities for amplification of the optical signals in optical circuits. In this thesis, two types of samples containing different waveguides were studied and measured (strip silicon waveguide, silicon nitride slot waveguide). Both were coated with erbium-doped aluminum oxide thin films, which were grown with plasma-enhanced atomic layer deposition technique. The focus of the following work was to find out how experimental parameters (e.g., signal wavelength, pump power, waveguide dimension and annealing effect) affect the possibility of the fabricated Erbium doped silicon devices to get optical signal amplification. The largest signal enhancement achieved in the strip waveguides examined in this work was 3.03 dB. Assuming more optimal initial propagation losses of 1 dB/cm, this result means no more than 0.47 dB loss. For the slot waveguides, the best result of signal enhancement was 1.1 dB in a 250 μm long waveguide, which means that it is possible to achieve small net gain with good quality slot waveguides. Our results showed potential of our Erbium doped silicon photonics to achieve net gain for various applications (e.g., inter-chip connection, bio-sensing).

Keywords: Silicon photonics, Erbium, Atomic layer deposition, Silicon waveguide, Optical amplification

AALTO-YLIOPISTO
SÄHKÖTEKNIIKAN KORKEAKOULU

DIPLOMITYÖN
TIIVISTELMÄ

Tekijä: Lasse Pakarinen

Työn nimi: Atomikerroskasvatettu Er_2O_3 signaalin vahvistuksessa piipohjaisissa valokanavissa

Päivämäärä: 01.06.2017 Kieli: Englanti Sivumäärä: 8+54

Elektroniikan ja nanotekniikan laitos

Professuuri: Mikro- ja nanoteknologia

Työn valvoja: Prof. Zhipei Sun

Työn ohjaaja: M.Sc. Anton Autere

Piifotoniikkaa voidaan käyttää laajasti eri sovelluksissa, sensoroinnista kokonaan optiseen signaalin käsittelyyn. Kuitenkin, on haastavaa toteuttaa aktiivisia komponentteja, kuten vahvistimia ja laserointia, piillä johtuen sen epäsuorasta energiavälistä. Erbiumin uniikit fysikaaliset ominaisuudet vahvistusmateriaalina ovat hyvin tunnetut, varsinkin kuituoptiikassa. Atomikerroskasvatus on puolestaan loistava tekniikka ohutkalvojen tarkkaan kasvatukseen lähes minkä muotoisille pinnoille tahaansa. Piifotoniikan, erbiumin ja atomikerroskasvatuksen ominaisuuksien yhdistäminen voi luoda uusia mahdollisuuksia optisten signaalien vahvistamiseen optisissa piireissä. Tässä diplomityössä on tutkittu ja mitattu kahta eri tyyppisiä valokanavia sisältävää näytettä (pii strip valokanavia ja pii nitridi slot valokanavia), jotka molemmat olivat päällystetty plasma avusteisella atomikerroskasvatus tekniikalla kasvatetulla erbium seostetulla alumiinioksidi ohutkalvolla. Työn tarkoituksena oli, selvittää miten kokeelliset parametrit (esim. signaalin aallonpituus, pumppausteho, valokanavien dimensiot ja lämpökäsittely) vaikuttavat valmistettujen Erbium-seostettujen piivalokanavien mahdollisuuteen tuottaa optisen signaalin vahvistusta. Suurin signaalin parantuminen tämän työn strip valokanavissa oli 3,03 dB. Teorian mukaisilla optimaalisilla etenemishäviöillä 1 dB/cm, tämä tulos tarkoittaa enää 0,47 dB vaimennusta. Slot valokanavien paras mitattu signaalin paraneminen oli 1,1 dB, 250 μm pitkällä valokanavalla, mikä tarkoittaa sitä, että hyvä laatuisilla piivalokanavilla on mahdollista saavuttaa pieni nettovahvistus. Tulokset osoittivat potentiaalia, että Erbium-seostettu piifoniikka voi saavuttaa nettovahvistusta erilaisille sovelluksille (esim. inter-chip-yhteyksille, bio-sensoroinnille).

Avainsanat: Piifotoniikka, Erbium, Atomikerroskasvatus, Piivalokanava, Valon vahvistaminen

Preface

This thesis work has been carried out in the Photonics group at the Department of Electronics and Nanoengineering at Aalto University.

I want to thank my supervisor Professor Zhipei Sun for giving me the opportunity to do this thesis in his group. I would also like to thank my advisor Anton Autere: Firstly for helping me to join Professor Zhipei Sun's group, and secondly for all the guidance during measurements and for helping me to keep this work on the right path. Extra thanks to him for helping me using Matlab to process the measurement data and to analyze the results.

Big thanks to John Rönn, who grown the samples for me and gave me a lot of answers and information with atomic layer deposition and annealing part. With the language and text, placing it correctly and in readable form, I received a lot of help from Ninni Paulin. I want to thank him very much also.

In addition I would like to say a huge thanks to my beloved daughters Melinda and Ronja. They have always been an ending in my philosophical thoughts about meaning of life, and therefore also the meaning of this thesis. I wish to express a big thanks to Jessica Tallqvist, the mother of my children who has helped in the daily life and thereby has given me time to make this thesis. Thanks also to everyone who has given me extra time by helping with the children so that I have been able to concentrate working on this thesis. Last but not the least, I am truly grateful to my mother Siiri Pakarinen, for altruistically coming a long way to help with the kids whenever needed, and also for supporting me in many ways during my studies.

Otaniemi, 01.06.2017

Lasse Pakarinen

Contents

Symbols and abbreviations

Symbols

$\mathbf{E}$	electric field
$\mathbf{H}$	magnetic field
$\mathbf{D}$	electric displacement vector
$\mathbf{B}$	magnetic induction vector
$\mathbf{J}$	current density
ρ	charge density
σ	conductivity of the material
c	speed of light in vacuum $\approx 3 \times 10^8$ [m/s]
ϵ	permittivity of the material
μ	permeability of the material
$\mathbf{S}$	Poynting vector
A	amplitude of the wave
ω	angular freguency
k	wave number
n	refractive index of the material
υ	phase velocity
h	Planck's constant $6.63 * 10^{-34} Js$
k_B	Boltzman's constant $1.380 * 10^{-23} VAs/K$
T	temperature
α	propagation loss

Operators

$\nabla \times \mathbf{A}$	curl of vectorin $\mathbf{A}$
$\mathbf{A} \cdot \mathbf{B}$	dot product of vectors $\mathbf{A}$ and $\mathbf{B}$
$\frac{\partial}{\partial t}$	partial derivative with respect to variable t

Abbreviations

ALD	Atomic Layer Deposition
ASE	Amplified Spontaneous Emission
CCD	Charge Coupled Device
EDFA	Erbium-Doped Fiber Amplifier
EDWA	Erbium-Doped Waveguide Amplifier
ESA	Excited-State Absorption
ETU	Energy-Transfer Up-conversion
LASER	Light Amplification by Stimulated Emission of Radiation
N.A	Numerical Aperture
NIR	Near-Infrared
OSA	Optical Spectrum Analyser
PC	Personal Computer
PEALD	Plasma-Enhanged Atomic Layer Deposition
PZC	Piezo Controller Unit
SE	Spontaneous Emission
SEM	Scanning Electron Microscope
SOI	Silicon-On-Insulator
TE	Transverse-Electric
TM	Transverse-Magnetic
WDM	Wavelength-Division Multiplexer

1 Introduction

In the past few decades, the world has changed with the development of the optical technology field, the development of semiconductor technology, and the use of the optical signal for transmission and processing of information, as well as the replacement of copper cable to optical fiber and the change of data from analog to digital. With these developments, the amount of data transfer and the need of fast processing have increased enormously. Gordon Moore published already in 1965 that the amount of transistors per chip will double every 18 months [1]. This is known as Moore's law and it is shown to be true up to the present days.

Optical fibers and fiber amplifiers, in particular, erbium-doped fiber amplifiers (EDFA), have mostly been the solution for need of data transmission in telecommunication [2]. Waveguides can combine optical components for optical circuits, similar to the way that microelectronics combines the electronic components for integrated circuits. They make it possible to leave off changing the optical signal into an electronic form and back to optical, which causes the slowness, complexity, increases the possibility of errors and additional costs. [3] Optical integrated circuits should have propagation loss as low as possible. There should be as few couplings as possible because they easily cause notable attenuations. However, the aim is to reach all-optical networks and data processing. [4]

One of the current application destinations is to develop more efficient and low-cost optical solutions into data centers. Today's optical devices are mostly fabricated from more exotic materials than silicon, such as indium phosphide (InP), gallium arsenide (GaAs) or lithium niobate ($LiNbO_3$). Compared to silicon, they are more complex to fabricate and relatively expensive. Optical technology to the mass market at this area may happen only if manufacturing can be high-volume and low-price. This could happen if it is possible to 'siliconize' photonics which means integration of multiple photonic circuits on a single silicon chip and Moore's Law would be really possible also to photonics. [5–7]

Silicon photonics has become an interesting and promising photonic integration platform during the last two decades. Silicon is an optimal material for electronics and it also has useful properties for photonics. [5,8] Because silicon's band gap is ~ 1.1 eV it is almost transparent to a wavelength range of 1300 nm - 1600 nm which is the most important and commonly used for fiber telecommunication. In addition, a high refractive index of the silicon creates a high index contrast surrounding the material and thus enabling smaller devices, which can be tightly bended. [9–11] However, it is challenging to use silicon to make active photonic devices, due to its indirect bandgap. Silicon has also some other disadvantages which hinder its use for photonics: for example, the problem to coupling light between silicon and other materials due to its high refractive index, and the problem to use as a nonlinear optical material [12]. Silicon based optical waveguides can be used for passive photonic devices (such as wavelength filters) to combine with active materials (such as rare earth oxides) for active photonic devices such as light emitters. Usually such devices are based on a simple silicon-on-insulator (SOI) waveguides. Very interesting ones are the strip and slot waveguides. During recent years the use of them have been demostrated in

all-optical signal processing. [7, 8]

The elements of the rare-earth metals have unique optical properties arising from their electron configuration. For example, they can emit light in a very narrow or wide bandwidth and emission can be controllable by the host materials. [13] The optical amplifier's gain material requires specific features. The main requirements are energy levels and their lifetimes which need to be suitable for stimulated emission at required wavelengths. Usability of the gain material also can be affected by their thermal characteristics, the available pump sources, as well as the existence of suitable host materials. Considering these features, Erbium is especially suitable for optical fiber amplifier applications. In particular there is an excellent match between the energy level and the minimum wavelength range of the commercial optical fiber. So the EDFA has become a significant part of the modern optical telecommunication networks. [2, 14] In silicon photonics the biggest loss is resulted by the coupling between the integrated circuit chips. Therefore it has attracted great interest to use the erbium as gain material in the micrometer range and for the development of erbium-doped waveguide amplifier (EDWA) [15]. But it poses great challenges to use erbium in very compact silicon integrated circuit chips. For example, erbium ion concentration must be much higher with reduced losses due to unwanted transitions. [16]

Atomic layer deposition (ALD) has been a popular deposition technique in the past few decades because it has excellent deposition properties [17]. For example, ALD can be utilized to grow atomically-thin films layer-by-layer on different types of surfaces with the exactly wanted composition. One of the important benefits particularly for integrated optical circuits is that ALD does not require any etching steps [18]. For these reasons, ALD is especially useful in semiconductor technology [12]. Recently, plasma-enhanced atomic layer deposition (PEALD) has been proposed, as it offers more freedom to choose the deposition parameters and provides an opportunity to deposit single-element ALD materials [19].

In conclusion, these properties of silicon, erbium and ALD together can create an opportunity to make ALD grown erbium doped film on the top of the waveguide area, which can be a part of the silicon optical circuit. For example, this can be combined with the devices that have already been fabricated e.g. modulators, splitters, couplers, Wavelength-Division Multiplexers (WDM) and so on [20, 21]. It would be possible to enable these devices to work as an amplifier for photonics, in spite of silicon's indirect bandgap. This possibility has inspired this thesis.

This thesis studied and measured two different kinds of silicon samples. One type of sample was a strip waveguide set which has four sets of different parameters, such as length and width. Another type of sample is slot waveguide, which has six sets of different parameters, such as length and slot width. Both types of samples are coated with 130 nm thick layer of PEALD grown Er/Al_2O_3. For this work, a custom-made measurement setup was built, which made it possible to measure both types of samples with different parameters. The signal wavelengths were selected in a range of interest gap between 1520 nm - 1570 nm, where erbium absorption and emission curves intersect [15]. Measurement arrangement was also possible to adjust the polarization to obtain as much as possible of a signal to go into the erbium doped

area of the waveguides. This meants for the strip waveguides TM polarization mode and for the slot waveguides TE-mode. In measurements the cut-back method was used to find out waveguide attenuation or amplification coefficient [22]. In addition, I solved out how annealing after ALD growth affects performance of strip waveguide samples. Because there were many waveguides and a lot of different measurement variations for each sample, there was also a lot of measurement data received and to be analyzed. At the same time, a large number of measured points helped to notice the quality errors and random errors, and thus excluded the unvalid measurements from the final analysis of the results. [23]

The purpose of this thesis was to find out if it is possible to achieve the net gain with ALD grown Erbium doped thin films. This thesis is arranged as follows: Basic theory about electromagnetic field, fibers, waveguides, attenuation and amplification is presented in Chapter 2. After that erbium (Chapter 3) and atomic layer deposition (Chapter 4) are presented. Chapter 5 illustrates the research methods and presentation of measurement setup. Chapter 6 contains results and their analysis. The last chapter presents the conclusions which have been made based on the results of the measurements.

2 Background and theory of optical fibers and waveguides

This section explains the fundamentals of the properties and behavior of electromagnetic waves, as well as principles of optical waveguides. In addition, the signal attenuation and amplification mechanisms in optical fibers and waveguides are explained. The signal attenuation and amplification are in a significant role in the optical transmission of information [24]. These are the main issues of this work and the results of measurements related.

2.1 Electromagnetic theory

Electromagnetic radiation carries energy. It propagates in successive waves which can be divided into electrical and magnetic parts. In 1873 James Clerk Maxwell described mathematically the behavior of the electromagnetic field and its interaction with materials. The Maxwell's equations described in differential form are

$$\nabla \cdot \mathbf{D} = \rho, \tag{1}$$

$$\nabla \cdot \mathbf{B} = 0, \tag{2}$$

$$\nabla \times \mathbf{E} = -\frac{\partial \mathbf{B}}{\partial t}, \tag{3}$$

$$\nabla \times \mathbf{H} = \mathbf{J} + \frac{\partial \mathbf{D}}{\partial t}. \tag{4}$$

Where $\mathbf{D}$ is the electric displacement vector, $\mathbf{B}$ is the magnetic induction vector, $\mathbf{E}$ is the electric field, $\mathbf{H}$ is the magnetic field, $\mathbf{J}$ is the current density, ρ is the charge density and t is the time. [25]

Electric or magnetic field can not exist by itself, they are dependent on each other. The fields are perpendicular to each other, the equations are congruent with each other and the change in electric field causes a change in the magnetic field and vice versa. The connection between the current density and the electric field can be presented $\mathbf{J} = \sigma\mathbf{E}$, where σ is the conductivity of the material. In addition, the vectors $\mathbf{D}$ and $\mathbf{B}$ are connected to the electric and magnetic field vectors in linear isotropic media by,

$$\mathbf{D} = \varepsilon\mathbf{E}, \tag{5}$$

$$\mathbf{B} = \mu\mathbf{H}. \tag{6}$$

where ε is the permittivity of the material and μ is the permeability of the material. These equations are called constitutive relations. The permittivity and permeability are defined as $\varepsilon = \varepsilon_0\varepsilon_r$ and $\mu = \mu_0\mu_r$, respectively. Here ε_0 and μ_0 are the vacuum permittivity and vacuum permeability and ε_r and μ_r are relative permittivity and permeability. Most dielectric materials are nonmagnetic, thus $\mu = \mu_0$.

Fields energy densities are given by

$$u_E = \frac{\varepsilon_0}{2} E^2, \tag{7}$$

$$u_B = \frac{1}{2\mu_0} B^2. \tag{8}$$

Electromagnetic energy flow S, which describes the energy passing through a surface per unit time is given by

$$S = \frac{1}{\mu_0} EB \tag{9}$$

Vector representation for energy flow is called the Poynting vector **S** and it can be presented as

$$\mathbf{S} = \frac{1}{\mu_0} \mathbf{E} \times \mathbf{B} = c^2 \varepsilon_0 \mathbf{E} \times \mathbf{B}. \tag{10}$$

where c is speed of light in vacuum. [3, 26, 27]

2.1.1 Light propagation

The electric field and the magnetic field oscillate relative to each other perpendicular to the plane that is described in Figure 1. The electromagnetic wave equation can be solved from Maxwell's equations. The wave equation for electric field in linear, isotropic and homogeneous media is

$$\nabla^2 \mathbf{E} - \mu\epsilon \frac{\partial^2 \mathbf{E}}{\partial t^2} = 0 \tag{11}$$

Due to the parallelism of fields and equations, a similar wave equation can be derived from the magnetic field

$$\nabla^2 \mathbf{H} - \mu\epsilon \frac{\partial^2 \mathbf{H}}{\partial t^2} = 0 \tag{12}$$

The simplest solution of these equations is the monochromatic plane wave

$$\psi = Ae^{-i\omega t} e^{i\mathbf{k}\cdot\mathbf{r}}, \tag{13}$$

where A is amplitude of the wave, ω is the angular freguency and $k = \frac{n\omega}{c}$ is the wave number. [28]

The speed of light is slower in the medium than in vacuum. The absolute refractive index of the material n is given by the phase velocity of the material $\upsilon = \sqrt{\frac{1}{\epsilon\mu}}$ in the relationship between the speed of light in vacuum

$$n = \frac{c}{\upsilon} = \sqrt{\frac{\varepsilon\mu}{\varepsilon_0\mu_0}}. \tag{14}$$

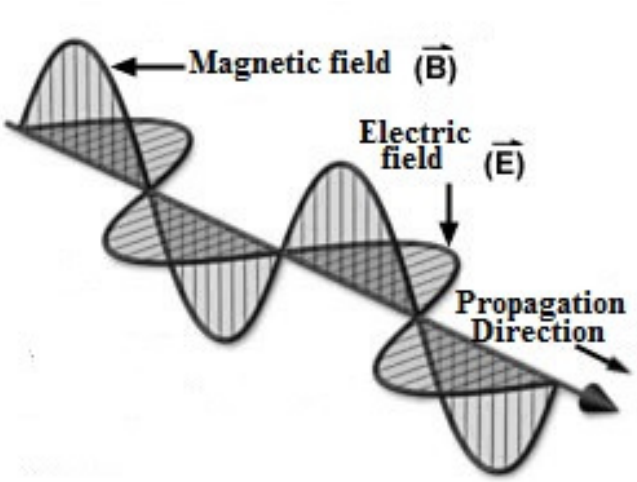

Figure 1: The electromagnetic wave propagation. [29]

As mentioned above, the materials that are used in optical fibers and wavequides are nonmagnetic ($\frac{\mu}{\mu_0} = 1$) so the refractive index can be written simply $n = \sqrt{\frac{\varepsilon}{\varepsilon_0}}$. The refractive index of the material is dependent on the wavelength, which is called material dispersion. In normal dispersion, shorter wavelengths are propagating slower than longer wavelengths, thus the materials refractive index decreases as wavelength increases. Material dispersion is discussed in more detail in section 2.1.5. So, refractive index of the material depends on two things, the characteristics of the material and the wavelength of the electromagnetic radiation. [30]

2.1.2 Reflection and refraction

French mathematician Pierre de Fermat presented in 1662 a principle which is now known as Fermat's principle. According to this principle, the light beam travels the distance between two points on the fastest route and, hence, rotate the areas of high refractive index of the inhomogeneous medium. The basic laws of light propagation arising from Fermat's principle. [30]

1. The light propagates in a straight line in a homogeneous medium.

2. The law of reflection is shown in Figure 2a. When the beam is reflected in the angle of incidence θ_1 equals the angle of reflection θ_2. In addition, the incoming beam, reflected beam and the normal of the reflection surface are in the same plane.

3. The law of refraction is shown in Figure 2b, also known as the Snell's law, according to this

$$n_1 \sin\theta_1 = n_2 \sin\theta_2, \tag{15}$$

where θ_1 is the angle of incidence, θ_2 is the angle of refraction and similarly n_1 and n_2 are the refractive indexes of different media. In addition, the beams and the normal of the surface are in the same plane.

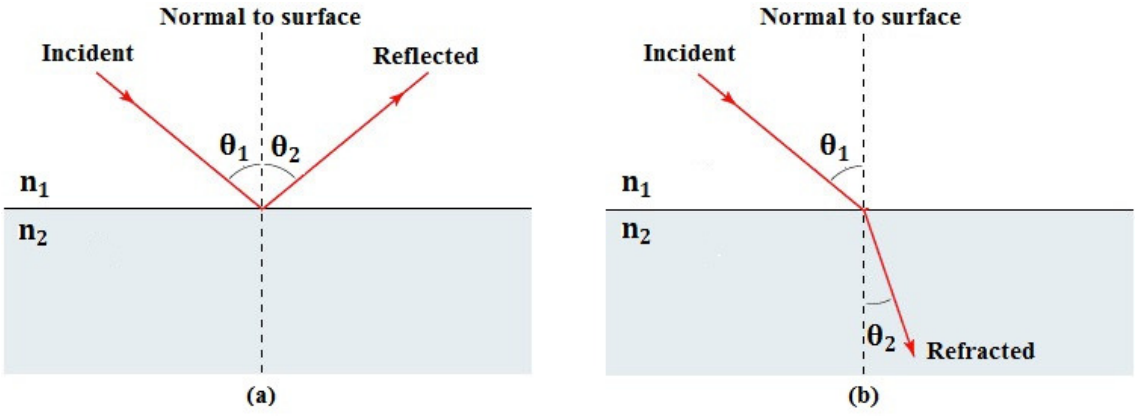

Figure 2: a) The light reflection and b) refraction.

Snell's law can lead to a critical angle when the beam passes through an optically denser media to optically less dense media, $n_1 > n_2$. The critical angle of the total internal reflection is obtained

$$\theta_c = \arcsin\left(\frac{n_2}{n_1}\right). \tag{16}$$

The total internal reflection and the critical angle are illustrated in Figure 3. When the incident angle is greater than θ_c, the incident wave is completely reflected, which is called total internal reflection (TIR). In TIR all of the optical power is reflected, however there exists also a transmitted field in the medium of lower refractive index called the evanescent field (or wave). Evanescent fields are not propagating and thus it does not transport energy from the interface, instead it is decaying exponentially into the medium with lower refractive index. Also, from Snell's law is derived a very important rule for how large an angle of light can be connected to the optical fiber or waveguide so that it does not escape from the core. If the light is connected to from the air, or $n_0 = 1$, the angles from Figure 4 and according to Snell's law can be calculated

$$n_0 \cdot \sin\theta_i = n_1 \sin\theta_r = n_1 \cos\theta_c = n_1\sqrt{1 - \left(\frac{n_2}{n_1}\right)^2} = \sqrt{n_1^2 - n_2^2}. \tag{17}$$

The angle of the resulting equation is called the numerical aperture. Usually in optical telecommunication applications, the relative refractive index difference $\Delta = \frac{n_1 - n_2}{n_1}$ is $\Delta \ll 1$ In this case, can be approximated

$$N.A. \approx n_1\sqrt{2\Delta}. \tag{18}$$

[32]

2.1.3 Polarization

From Maxwell's equations follows that in homogeneous and linear medium, the electromagnetic radiation has a only transverse polarization. Plane wave is obtained

$$i\mathbf{k} \cdot \mathbf{E_0} e^{i(\mathbf{k}\cdot\mathbf{r} - \omega t)} = 0, \tag{19}$$

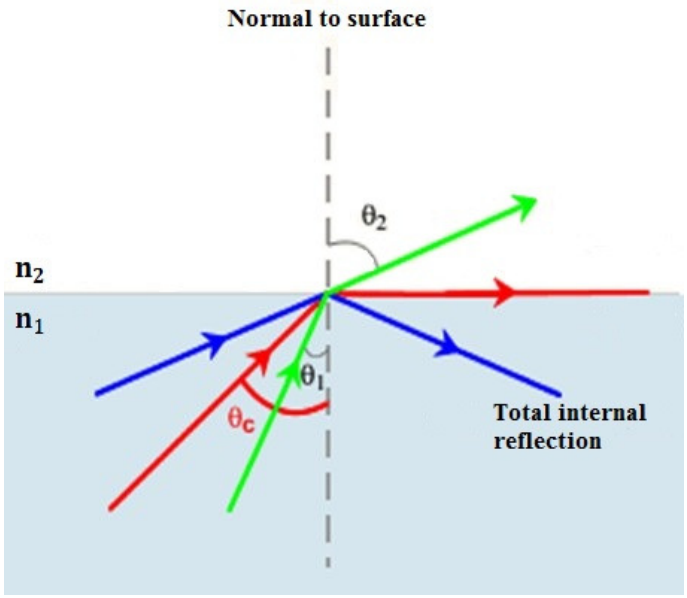

Figure 3: The total internal reflection and the critical angle θ_c. [31]

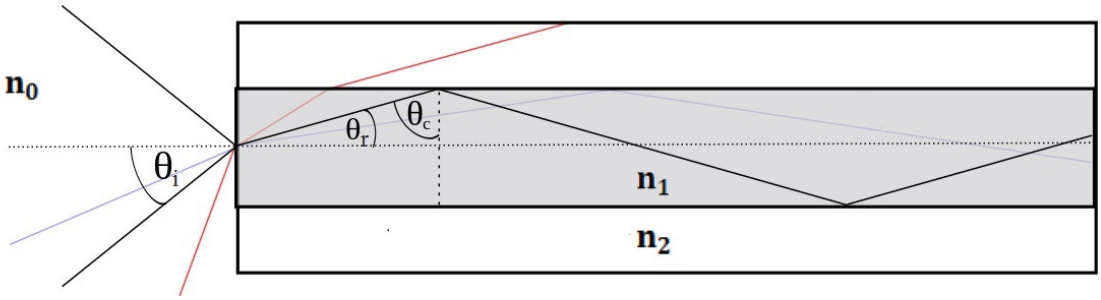

Figure 4: Description of the numerical aperture and the important angles.

On the basis of Equation 19 have to be $\mathbf{k} \cdot \mathbf{E_0} = 0$ and both electric and magnetic field oscillation is therefore perpendicular to the direction of propagation of radiation.

The electric field of linearly polarized light oscillates in a certain plane, this is illustrated in Figure 5. If the polarization direction is in the plane of incidence, it is called the p-polarized or commonly it is referred to as transverse-magnetic TM polarization. If the polarization is perpendicular to the plane of incidence it is called s-polarized or it also called transverse-electric TE polarization. Elliptically polarized light is obtained when the combined level of two mutually perpendicular polarized plane waves are in such a way that the waves are equal to a phase shift some angle φ. If $\varphi = \frac{\pi}{2}$ and $\mathbf{E}_{0x} = \mathbf{E}_{0y}$ obtained by circularly polarized wave. The circularly polarized wave shows the front view so that a constant electric field absolute value rotate either counterclockwise (+) which is described in Figure 6 or clockwise (-). [28, 30]

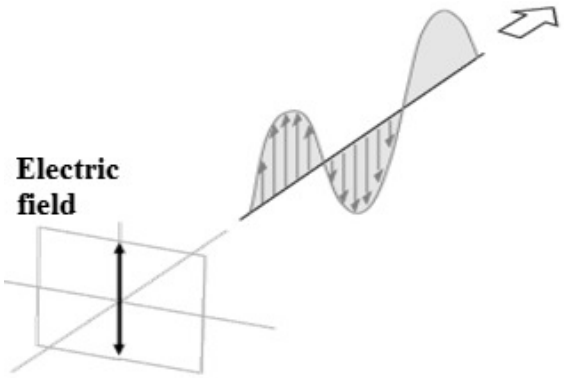

Figure 5: The electric field of the linearly polarized electromagnetic wave. [30]

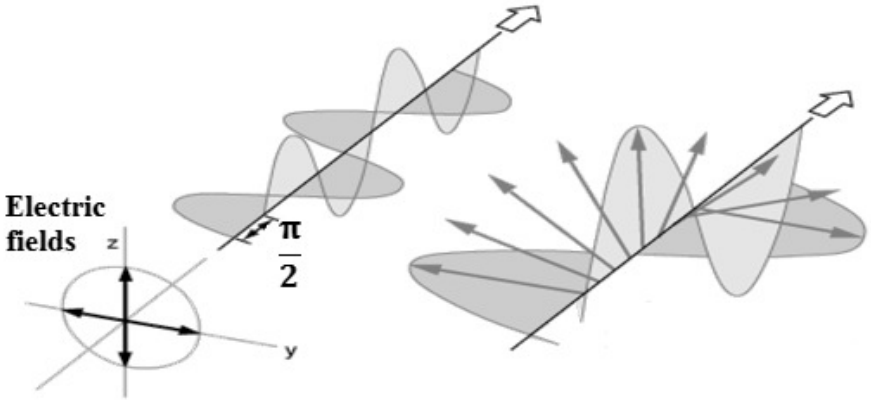

Figure 6: Description of the electric fields of the counterclockwise circularly polarized electromagnetic wave. [30]

2.1.4 Dispersion

The dispersion means basically that electromagnetic wave packet broadening of the fiber or waveguide. Its different mechanisms of occurrence are modal dispersion, chromatic dispersion and polarization mode dispersion.

The modal dispersion occurs only in multi-mode optical fibers. It means propagation delay between a shorter and a longer modal distance difference to go in the fiber. The modal dispersion does not of course occur in single-mode fibers.

Chromatic dispersion consists of material and waveguide dispersion. Material dispersion due to the refraction index of the medium changes with the wavelenght. The waveguide dispersion means that different wavelenghts have different delays. Chromatic dispersion parameter of the normal communication optical fiber for the wavelength dependence is described as figure 7. The zero point of the dispersion λ_{ZD} can be moved by making a zero dispersion-shifted fiber.

In single-mode fiber polarization mode dispersion also occurs [30]. Surface geometry and mechanical stresses may cause that different polarization modes can

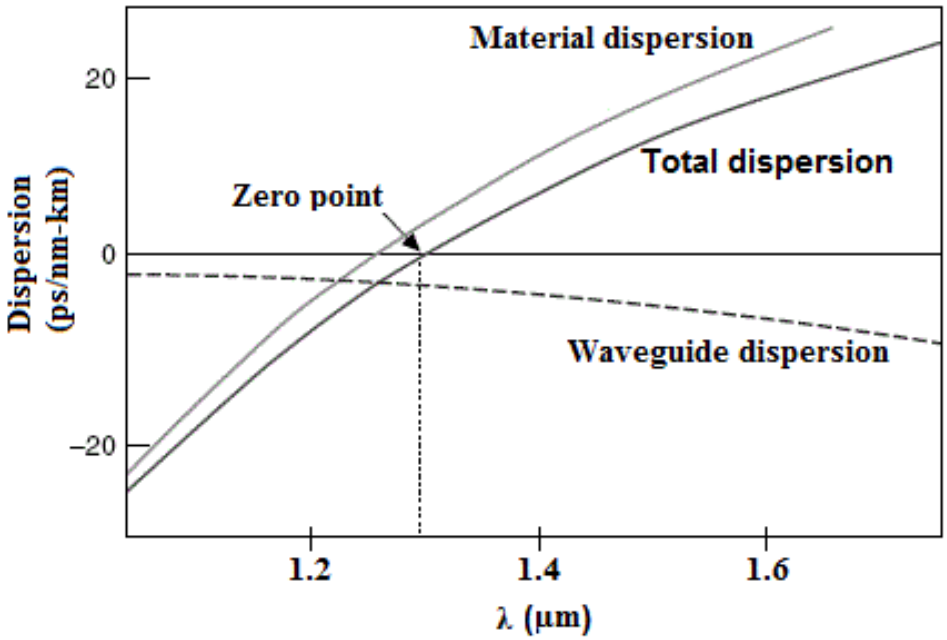

Figure 7: The chromatic dispersion in normal step-index single-mode fiber. The zero point of chromatic dispersion is near of 1.3μm. [30]

have different phase and group velocities. [33]

2.2 Optical fibers and waveguides

The optical fibers are usually prepared of very pure silica. Figure 8 shows a typical fiber cross-sectional profile. The fiber consists of a core and a cladding, and usually a plastic coating. The core refractive index n_1 is slightly higher than in the ambient cladding n_2. [4]

A planar slab waveguide is the simplest one of waveguide structures. It has a higher refractive index of the film n_f, which is surrounded by layers of lower refractive index materials. The layer below the film it is called the substrate n_s and layer on top of the film similarly a cover n_c. A slab waveguide is symmetric if $n_s = n_c$, and otherwise asymmetric. Figure 9 is an example of a simple slab waveguide structure in which the substrate is silicon dioxide, the film material is silicon and the cover is air. This kind of wavequide is typically called as Silicon-On-Insulator slab wavequide (SOI). [11] Cross-section of the different kinds of the waveguide is presented in Figure 10, where refractive indexes of the imaged structures are selected such that the $n_1 < n_3 < n_2$ [34].

Going through a bit more specifically details of the strip and the slot waveguide, because in this work, the measured waveguides were four sets of strip and six sets of slot waveguides, these are shown in detail in Figures 30 and 31.

Strip waveguides are rectangular waveguides which geometry offers good confinement in vertical as well as horizontal directions. The propagation modes in strip

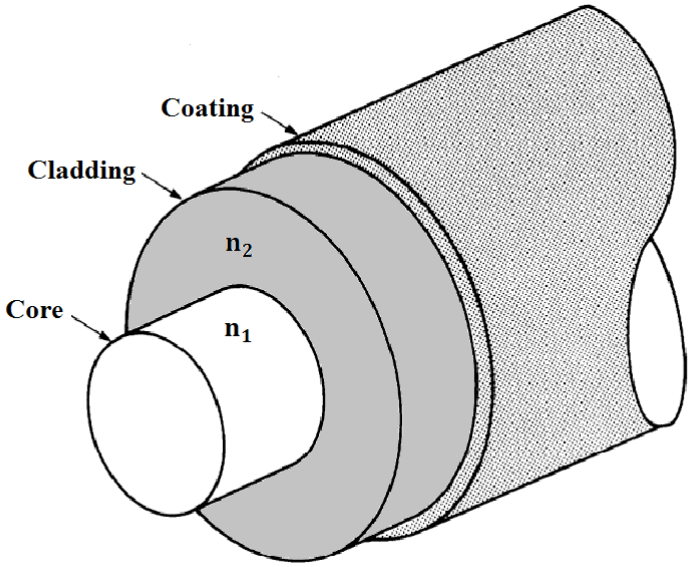

Figure 8: The typical cross-section of the optical fiber.

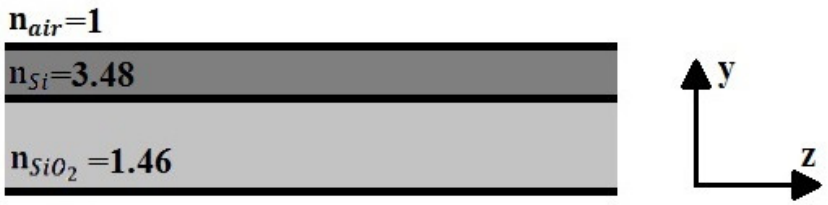

Figure 9: The simple Silicon-On-Insulator slab waveguide.

waveguides can be set so that the evanescent field can be relatively strong at the waveguide surfaces, such as the electric field distribution in the strip waveguide with TM-polarization mode in Figure 30 can be seen. So cladding material properties can be exploited and therefore strip waveguide made silicon-on-insulator is very suitable for silicon photonics applications. [17]

The slot waveguide structure provides a larger part of the electromagnetic field to go in low refractive index material. The structure and distribution of the field are different. The structure can be thought that the field is caused to propagate in the narrow gap between two strip waveguides, so-called slot. [35] Because the effects of cladding material can be bigger, it will make silicon photonics platform even more interesting. But due to their complex structure, their manufacture is a bit more difficult. [17]

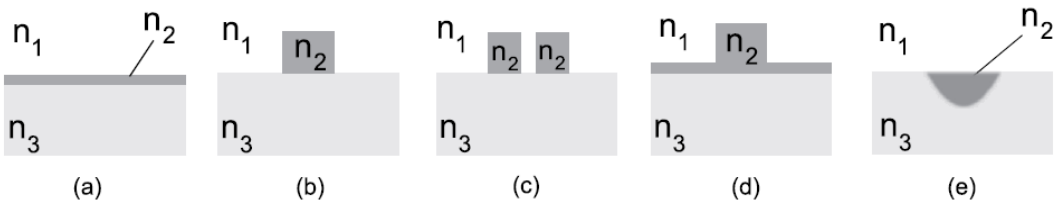

Figure 10: Illustration of waveguide structures: (a) slab waveguide, (b) strip waveguide, (c) slot waveguide, (d) ridge waveguide and (e) diffused waveguide. [34]

2.3 Attenuation

In waveguides, the key issue is the signal attenuation. Attenuation is defined as loss of optical power in a specific way of a fiber or waveguide. The attenuation coefficient α is typically obtained by the formula

$$\alpha = -\frac{1}{L} \ln \frac{P_{out}}{P_{in}}, \tag{20}$$

where L is the length of the fiber or waveguide, P_{in} is the input optical power and P_{out} is the output optical power of the fiber or waveguide. Attenuation is usually expressed in decibels per distance, in which case it be calculated using the formula [30]

$$\alpha_{dB} = -\frac{10}{L} \log \frac{P_{out}}{P_{in}}. \tag{21}$$

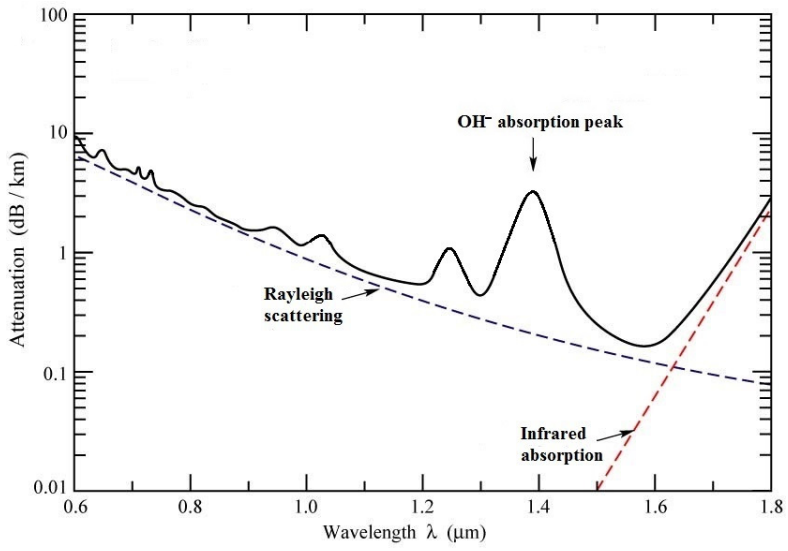

Figure 11: Schematic illustration of typical attenuation spectrum of the optical fiber.

Typical attenuation of optical fiber with SiO_2 core, is shown as a function of wavelength in Figure 11. Nowadays it is possible to produce fibers with lower

impurity-induced losses, such as those of the OH^- -absorption peak can be removed completely, also called a water peak. [36] Nowadays, the attenuation is mainly due to the light absorption and different scattering processes. Rayleigh scattering is the most dominant scattering process, it is due to inhomogeneities, whose size is much less than the wavelength, in the core. Rayleigh scattering is accounted for about 96% of the total scattering losses and the remainder consisting of Mie, Raman and Brillouin scattering. [30]

2.3.1 Scattering losses

In waveguides propagation losses are mainly due to the sidewall surface roughness which leads to scattering losses. In addition, leakage through the buried oxide into the substrate, particularly if the optical field is not guided sufficiently, may cause additional losses. Typically, silicon based strip waveguide losses are in an order of 1 dB/cm, and slot waveguides 4 dB/cm. [37, 38] Figure 12 is a scanning electron microscope (SEM) image that shows illustratively the sidewall surface roughness of a SOI slot waveguide.

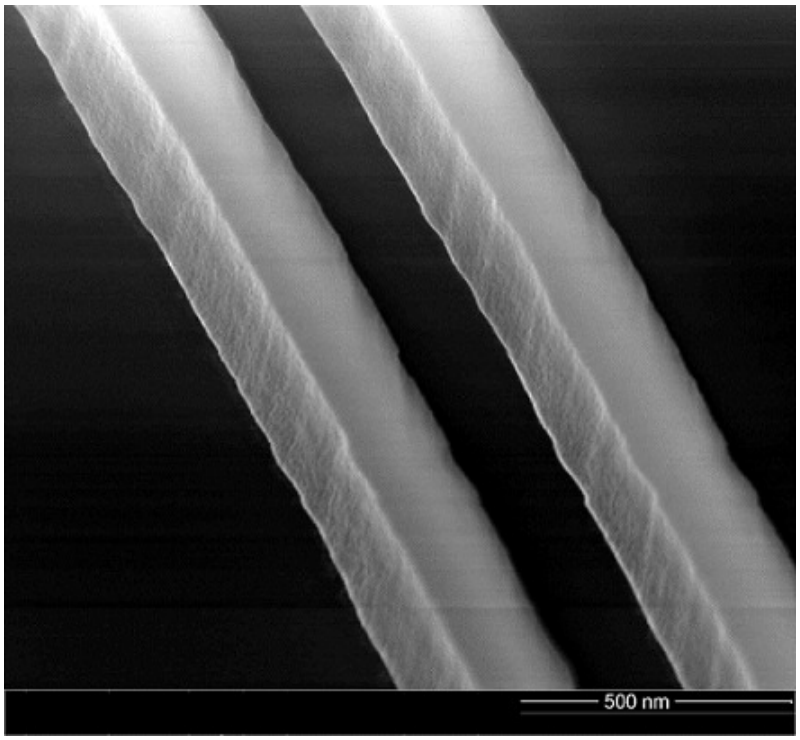

Figure 12: SEM image of a SOI slot waveguide.

2.3.2 Absorption losses

The wavelength range of a waveguide is decided by transparency of the material by which the waveguide is fabricated. For example in normal silica based optical fibers the wavelength is around 1550 nm since the absorption losses are the lowest

at that wavelength. Since silicon is a semiconductor with 1.12 eV ($\sim$ 1100 nm) bandgap, the wavelength in silicon waveguides must be larger than 1100 nm to avoid absorption loss of the propagating light. Silicon nitride is an alternative for silicon for applications in the visible range of the spectrum. It is a wide bandgap semiconductor ($\sim$ 5 eV) and thus is transparent from visible to IR. However, the refractive index of silicon nitride is lower than that of silicon, which reduces the index contrast between the core and cladding. The refractive indices of silicon and silicon nitride can be seen in Figure 13a. The imaginary parts of the refractive indices, corresponding to the absorption in the material, are shown in Figure 13b and 13c, respectively.

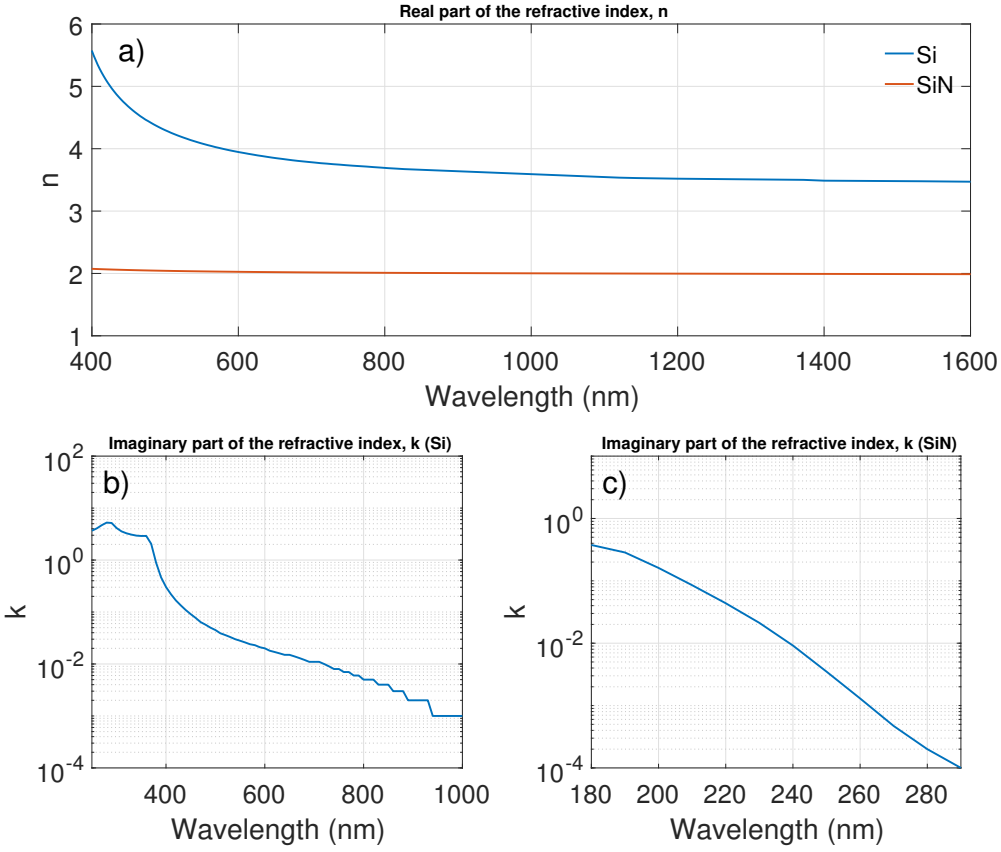

Figure 13: Refractive indexes of Silicon and Silicon nitride. a) Real parts of the refractive indicies. b) Imaginary part of the refractive index of silicon. c) Imaginary part of the refractive index of silicon nitride. [39]

2.4 Amplification

Albert Einstein showed in 1917 that the interaction of electromagnetic radiation and matter requires a previously unknown stimulated emission process to exist. Electromagnetic radiation have the photon energy which can be expressed as a mode

of frequency ν is

$$E = h\nu \tag{22}$$

where $h = 6.63 \times 10^{-34} Js$ is Planck's constant.

If the photon energy is sufficiently large, then due to absorption the electron moves into a higher energy state. The electron can return back to its ground state by spontaneous emission, whereupon energy is released in the form of photon. This release of the photon are random in direction and phase. The excited electron release can also be affected. Released photons have the same direction and phase. This process is called stimulated emission and makes it possible to light signal amplification for LASER. LASER is an abbreviation of the Light Amplification by Stimulated Emission of Radiation. Absorption, spontaneous emission and the stimulated emission are illustrated in Figures 14, 15 and 16. [40, 41]

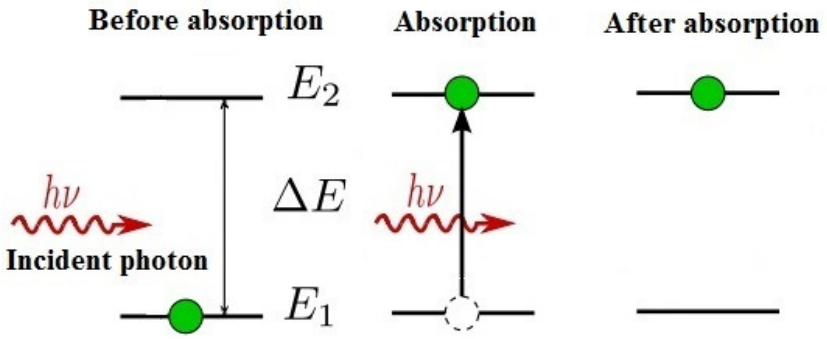

Figure 14: Classic description of the absorption.

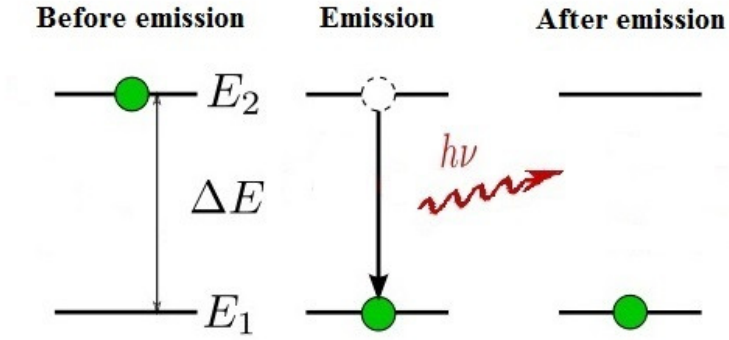

Figure 15: Classic description of the spontaneous emission.

Due to thermal equilibrium, most of the electrons of the substance is in a ground state E_1. Distribution of electrons between the ground state and the excited state E_2 complies with the Boltzman distribution.

$$\frac{N_2}{N_1} = e^{-\frac{(E_2 - E_1)}{k_B T}}, \tag{23}$$

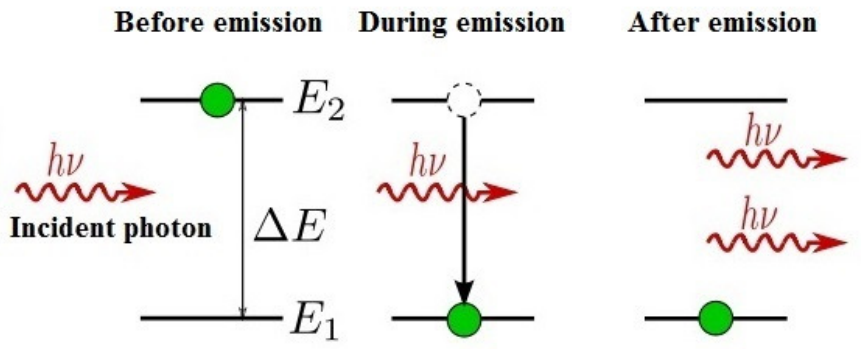

Figure 16: Classic description of the stimulated emission.

where N_1 and N_2 are the number of electrons in the ground state and the excited state, $k_B = 1.380 \times 10^{-23} VAs/K$ is Boltzman's constant and T is temperature. In accordance with Einstein's indication of the absorption, spontaneous emission and stimulated emission are connected. From the excited state to the ground state the electron can move either through simulated emission or spontaneous emission, and in the other direction only with absorption. The spontaneous emission frequency is proportional only to the excited state occupation of N_2. The stimulated emission frequency is proportional to the excited state occupation N_2 and the density of the radiation field ρ_ν at a frequency ν. So-called stimulated absorption frequency is proportional to the density of the radiation field ρ_ν frequency ν and the number of ground state electrons N_1. In addition, the processes associated with their own Einstein coefficients as shown in Figure 17.

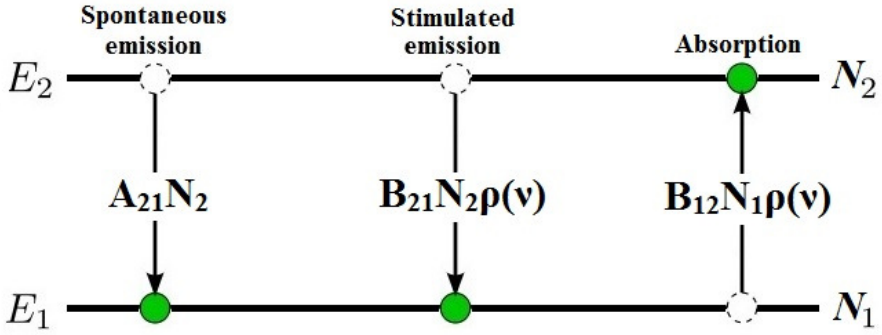

Figure 17: Transitions dependencies and Einstein coefficients.

In thermal equilibrium radiation emission complies with the black body radiation. Planck's law gives black body radiation density distribution as ρ_ν a function of

frequency ν.

$$\rho_\nu = \frac{8\pi h\nu^3}{c^3} \frac{1}{e^{\frac{h\nu}{k_B T}} - 1}, \tag{24}$$

From equations 24 and 25, as well as Einstein coefficients A_{21}, B_{21} and B_{12} from Figure 17 is obtained

$$\frac{A_{21}}{B_{21}} = \frac{8\pi h\nu^3}{c^3} \tag{25}$$

and

$$B_{12} = B_{21} \tag{26}$$

From these results it can be concluded that the Einstein coefficients A_{21}, B_{21} and B_{12} depend on each other. When one is known the other one can be calculated. The stimulated emission and absorption processes are opposite, because the stimulated emission coefficient B_{21} and the absorption coefficient B_{12} are equal. However, it is important to note that the change time of the population rates is not the same. Light can be amplified by stimulated emission as much electrons are in excited state. In fact, amplification occurs only when absorption is dominated by stimulated emission and that requires a large amount of electrons in excited state in order to form a population inversion between the excited state and the ground state.

The population inversion means that the excited state has more electrons than the ground state. The electron excited state does not last very long, usually only microseconds. Therefore the population inversion is best achieved by using three- or four-level systems, where the popular inversion condition is met between intermediate level and the ground state or between two intermediate levels. The basic principles of three- and four- level systems are shown in Figure 18. Thus, the top level must be tuned to get a lot of electrons. This is achieved by a so-called pumping, for example, optically, electrically or chemically. For optically it can be done by the pump laser. From top level electrons descend to the intermediate level, where they remain for longer. Actually, from equations 24, 25 and Einstein coefficients A_{21}, B_{21} and B_{12} it can be deduced that by optical pumping in two-level system, it is possible to reach only a situation of $N_1 = N_2$. In addition the system must be kind of that the energy difference between these levels to be quantified in ΔE is equal to that photon energy which is considered to amplified wavelength. [40, 42, 43]

Without changing the optical signal into an electric signal, every techniques for amplifying an optical signal, and the different types of amplifiers used by all in some way for the benefit of stimulated emission phenomenon. Different amplifiers have different characteristics and are used based on suitability, quality and price for different purposes. A variety of common optical signal amplifiers are semiconductor optical amplifiers (SOAs), erbium-doped fiber amplifiers (EDFAs) and Raman amplifiers.

Semiconductor optical amplifiers are structurally heavily doped pn-junctions. Pumping to the stimulated emission is achieved across the joint coupled to the forward voltage. Between the pn junction formed by the active region where the

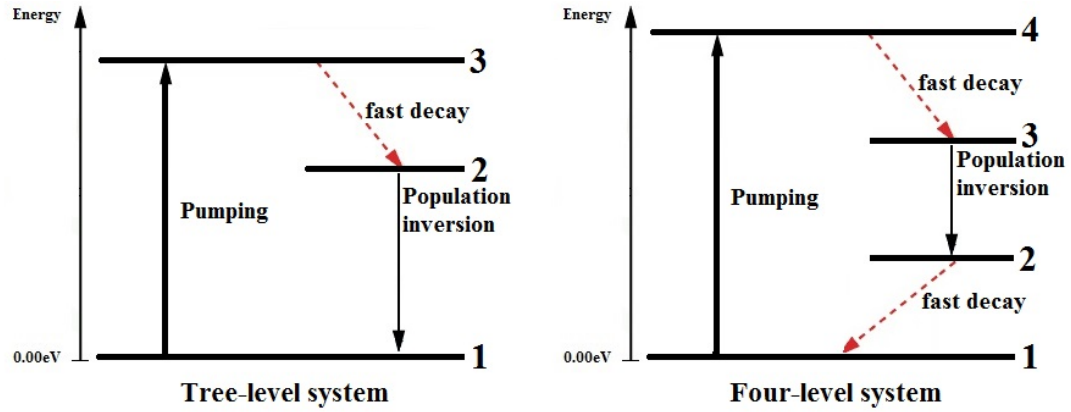

Figure 18: The basic principles of three- and four- level systems.

wave forms can be amplified. Semiconductor optical amplifiers can be prepared for all necessary optics telecommunication wavelengths, and in addition they are quite an efficient and cheap solution for amplifiers. The problems they pose are a confirmation polarization dependence and very fast response time, which causes non-linear distortion. [44]

EDFA is a fiber optic main amplifier, because it operates at a wavelength of 1550 nm, and as shown in Figure 11 and previously seen, this wavelength have also the minimum attenuation point of the optical fiber [45]. More specifically erbium optical properties are presented in the next chapter.

Raman amplifiers utilize a non-linear process caused by Raman scattering. Photon energy causes the molecules beneath phonons and this vibration can produce vibration or quantum phonon. Phonon excitation may cause the molecule to a higher energy state and when returning back to a lower energy level the molecule release energy in the form of a photon. Using the right kind of pump laser can achieve stimulated Raman scattering, which can amplifies the optical signal. [46]

3 Erbium

This section describes the elemental erbium, in particular its interesting and unique optical properties.

3.1 Basic information of Erbium

Erbium is an element on the periodic table with atomic number 68. The placement of the Erbium in the periodic table can be seen in Figure 19 and its basic features are presented in Table 1. Erbium belongs to the group of lanthanides including the periodic table of the elements 57-71. Lanthanides are shown in Figure 19 together with the actinides elements 89-103. Together with the scandium and yttrium all lanthanides belongs to so-called rare-earth metals but actually they are not so rare. The name "rare-earth metals" is really a historical relic of a time when they were difficult to identify and separate. However, erbium is also like other rare-earth metals, it cannot be found alone. They are always part of some minerals and their separation has been difficult before the ion-exchange methods were invented. Lanthanide's electron configuration is a different type than other elements and makes them so interesting and different behavior. From lanthanides neodymium Nd-60 and ytterbium Yb-70 are also optically interesting and useful. [2, 47, 48]

Table 1: The basic characteristics of erbium. [50]

Symbol	Er
Discovery date	1843
Discovered by	Carl Gustav Mosander, Sweden
Group	Lanthanides
Period	6
Block	f
Atomic number	68
Atomic weight	167.259
State at 20°C	Solid
Electron configuration	$[Xe]4f^{12}6s^2$
Melting point	1529°C, 2784°F, 1802K
Boiling point	2868°C, 5194°F, 3141K
Density (g cm^{-3})	9.07
Key isotopes	^{166}Er
CAS number	7440-52-0

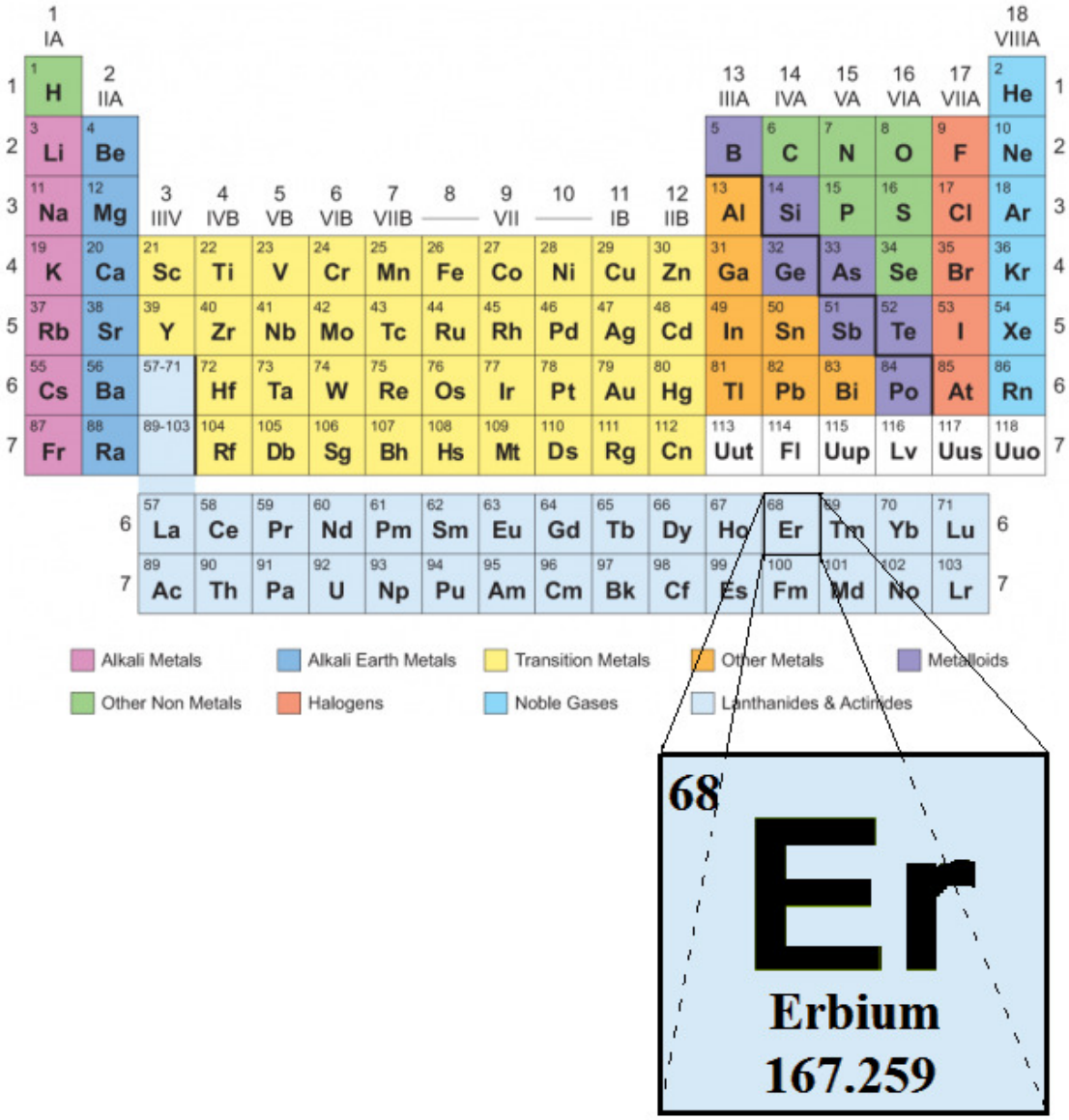

Figure 19: The periodic table of the elements and the place of Erbium. [49]

3.2 Optical properties of erbium

According to the classical model of an atom, the atom is a positively-charged nucleus surrounded by negatively-charged electrons. The electron shells fill in the order from lowest to highest energy and according to the distance of the shells. The valence electrons are on the outermost shells and react firstly. Lanthanides, this model is no longer valid, because the highest energy shell has shrunk into the previous shells. The electronic configuration of erbium is $1s^2 2s^2 2p^6 3s^2 3p^6 3d^{10} 4s^2 4p^6 4d^{10} 5s^2 5p^6 4f^{12} 6s^2$, which are often presented in the form $[XE]4f^{12}6s^2$, where [XE] is the core of the xenon. Erbium generally appears in its trivalent state Er^{3+}, since the ionization energies of 6s and one 4f electrons are so low. Then the electronic configuration

of the form [XE]4f^{11} and 4f state are the valence electrons of the Er-ions. 4f shell distance is almost twice as small as the average radii of the fully-occupied 5s and 5p orbitals. Therefore, the valence electrons are shielding 5s and 5p electrons behind. This shielding of the valence electrons is the reason for good optical properties of the lanthanides. [2, 13, 50]

The optical amplifier's gain material requires specific features, the main requirements are energy levels and their lifetimes which need to be suitable for stimulated emission at required wavelengths. Figure 20 illustrates the three lowest energy bands, ${}^4I_{15/2}$, ${}^4I_{13/2}$ and ${}^4I_{11/2}$, of Er^{3+} ions. Based on electrons relaxation times between ${}^4I_{11/2} \rightarrow {}^4I_{13/2}$ and ${}^4I_{13/2} \rightarrow {}^4I_{15/2}$, it can be seen that for the intermediate level ${}^4I_{13/2}$ a population inversion formed quite easily. Erbium has a feature to achieve the population inversion at a bandgap that produces photon emission at a wavelength of around 1550 nm. Erbium has an excellent match between the energy levels and the minimum wavelength range of the commercial optical fiber. That is the reason why the EDFA has become a significant part of the modern optical telecommunication networks. In addition to erbium the good available pump sources exist. Diode lasers at 980 nm and 1480 nm operating wavelength can be used for pumping. [2, 14] Usability of the gain material also can be affected by their thermal characteristics, as well as the existence of suitable host materials. For erbium, there are a lot of good hosts that meet the requirements of host materials, for example SiO_2, Al_2O_3 and Y_2O_3. [51]

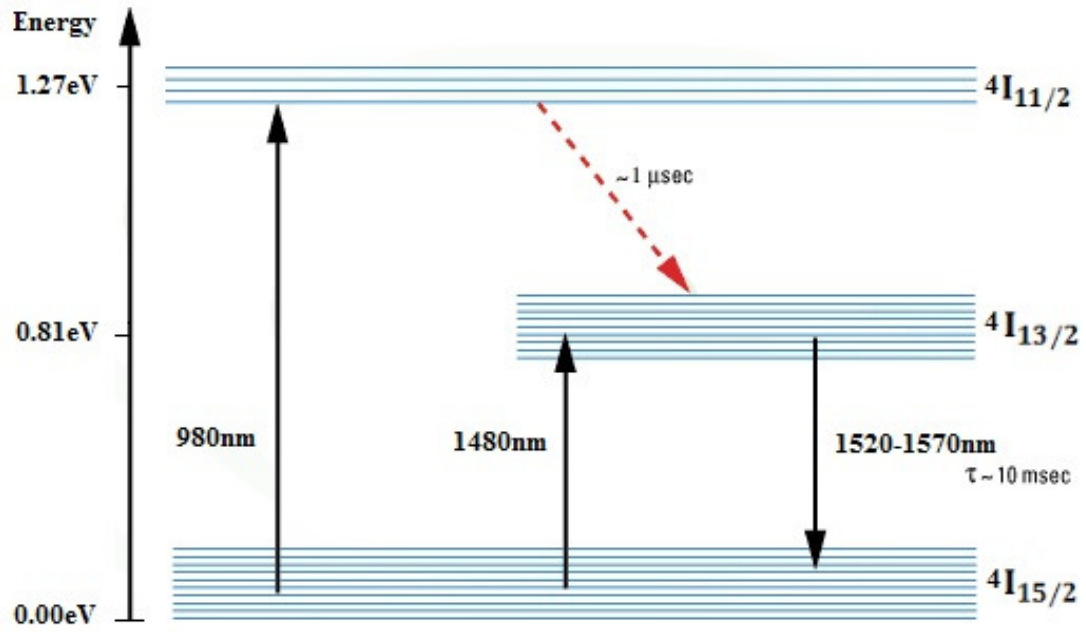

Figure 20: Three lowest erbium's energy bands.

Erbium's absorption and emission spectra of the ${}^4I_{15/2} \leftrightarrow {}^4I_{13/2}$ transition are show in Figure 21. This figure shows the spectra are rather wide. This is due to the fact that there are a lot of allowed transitions between the first excited state ${}^4I_{13/2}$ and the ground state ${}^4I_{15/2}$ as the energy band ${}^4I_{13/2}$ is split into 7 energy

levels. Also in this figure, it can be observed that the absorption and emission curves intersect at about the wavelength of 1530 nm and at 1550 nm point emission clearly dominates. [13, 15]

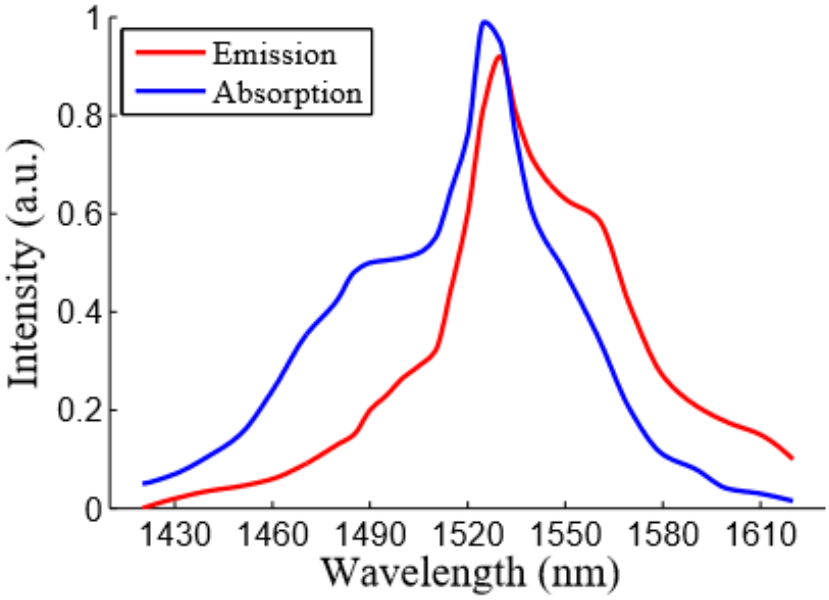

Figure 21: Erbiums absorption and emission spectra between energy levels ${}^4I_{15/2} \leftrightarrow {}^4I_{13/2}$ in Er-doped silica glass. Data from [15].

Figure 22a show a erbium's seven lowest energy bands, their life times and the corresponding wavelengths in Er-doped silica glass. In addition to these transitions, harmful transitions exists for using erbium as a gain material at around 1550 nm wavelength range. These unwanted transitions are the fact that the excited ions interact with prior to their desired stimulated emission. Ions are excited for the second time at the higher energy states and/or ions released transitions which emit light at a different phase and wavelength than the desired stimulated emission. These unwanted transitions as shown in Figure 22b.

Up-conversions of light occur when the sequential absorption of more than one photons leads to the emission of light at shorter wavelength than the excitation wavelength.[6] Figure 22b show a two-type of energy-transfer up-conversion (ETU). ETU1 occurs between two ions in the first excited state ${}^4I_{13/2}$ [11]. ETU2 occurs in the second excited state ${}^4I_{11/2}$ where the ions are pumped when using 980 nm pump wavelength. [15,51] Second type of up-conversion transition is the excited state absorption (ESA) and it occurs when the ions that already have the upper-bands can be excited again by absorbing a second pump photon in the process. [13]

In addition, spontaneous emission (SE) occurs when an ion spontaneously decays from excited state to ground state, which leads to a noise in the amplifier. Spon-

taneously emitted photons have random phase and energy, which corresponds to the energy difference between the energy states. [2] If spontaneous emission occurs between ${}^4I_{13/2}$ and ${}^4I_{15/2}$, the amplifier can amplify these spontaneously emitted photons. This process is shown in Figure 22b the amplified spontaneous emission (ASE) and it also leads to extra noise in the amplifier. [14]

The importance and meaning of these harmful transitions for effect of amplification of the light will increase when the pump power has to increase and/or the Er-concentration have to increase. Therefore, the unwanted transitions effect can be large, especially in the short millimeter range of waveguide amplifiers. [15, 16, 20]

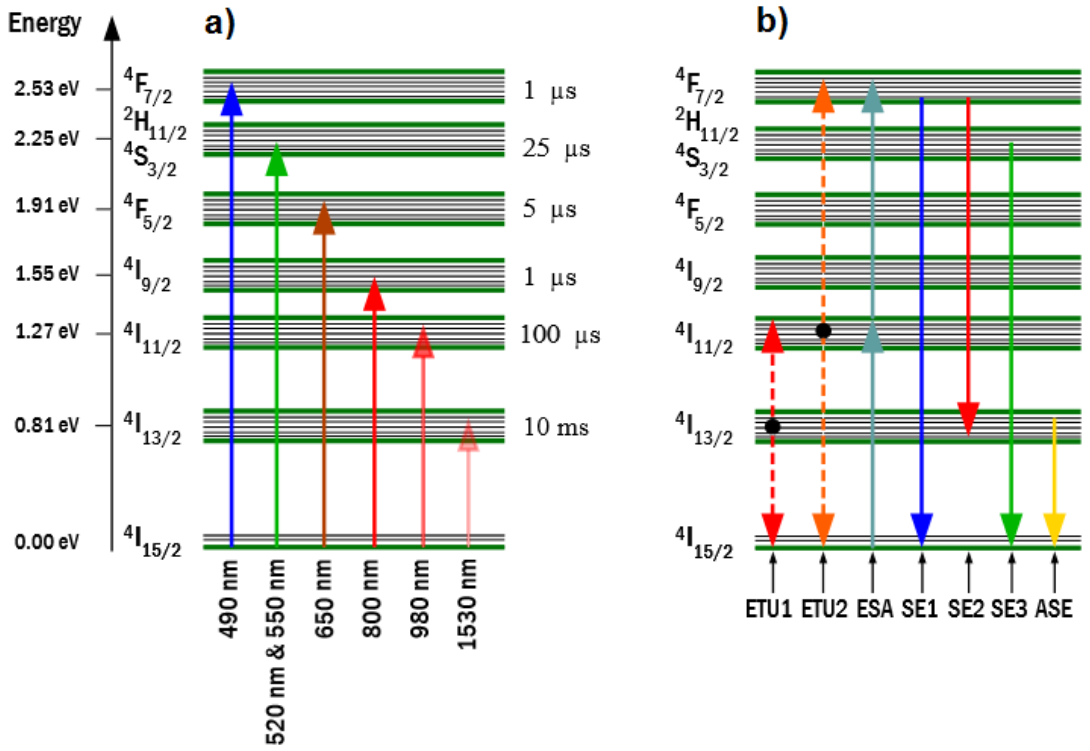

Figure 22: a) The erbium's seven lowest energy bands, their lifetimes and the corresponding wavelengths in Er-doped silica glass. b) The unwanted processes of Er-doped amplifiers. The processes are: energy-transfer up-conversion (ETU), excited-state absorption (ESA), spontaneous emission (SE) and amplified spontaneous emission (ASE) [21]

4 Atomic layer deposition

Atomic layer deposition (ALD) method was developed in Finland in 1977. It is a chemical vapor phase deposition (CVD) method that can produce thin films with excellent quality [52]. Since then, ALD has become a popular method for of thin film deposition, due to its unique deposition properties, such as high conformality, aspect ratio, and non-uniformity [53]. ALD is well suited in the semiconductor industry because it can be used to coat very high aspect ratio, nanometers-sized structures conformally. ALD's major advantage is that it can grow exact material composition of the monolayer by monolayer high-quality thin film evenly all form surfaces and also on top of complex structures without any kind of lithography steps. Therefore ALD is very popular especially for silicon photonics. [12, 17] In addition, compared to other vapor phase techniquis ALD's moderate growth temperature enables the use of integrated circuit structures to deposit high-k gate oxides [54]. Particularly ALD is a potential method for the production of erbium-based materials. As previously explained erbium already has a very important role in the amplification of optical signals.

4.1 Process and operation principle

ALD is a vapor phase technique, the operation is based on the sequential use of a gas or vapor phase chemicals. As distinct from other similar techniques, different precursor gases are pulsed into the reactor separately. Thus obtained a unique self-limiting film growth mechanism. [55] Four main steps of the basic operation cycle of ALD are shown in Figure 23. The deposition temperature is typically 100°C-300°C but in some processes it can be as high as 500°C. The purging is done using an inert gas to remove both the reactant that did not react with the substrate surface. Typically, the inert gas is N_2 or Ar. After cycling, shown in Figure 23, the result is a molecular monolayer of the material that was chemically produced from the two reactants. The second purge step remove remaining chemicals and by products. The deposition then continues to repeat this cycling procedure until desired film thickness is achieved. [52]

Thanks to this unique rotation process with ALD, it can deposit very exact and thin layers. On the other hand this method is very slow compared to other thin film techniques.

The deposition rate indicated in the most cases is around Å/cycle and one cycle deposition can increase up to 1Å layer. Deposited layer thickness depends on the deposition parameters. Deposition Process parameters can and must be optimized for different materials separately. The main parameters that affect the ALD rate and the layer thickness are the temperature throughout the process, the first precursor pulse time, purge time and flow rate, as well as another precursor pulse time, purge time and flow rate. The whole process temperature is the most important because different materials have different temperature range where growth can be predicted and can be utilized in ALD's unique features. This is called the ALD-window of the material. Growth layers are also based on the reactivity of the chemicals that

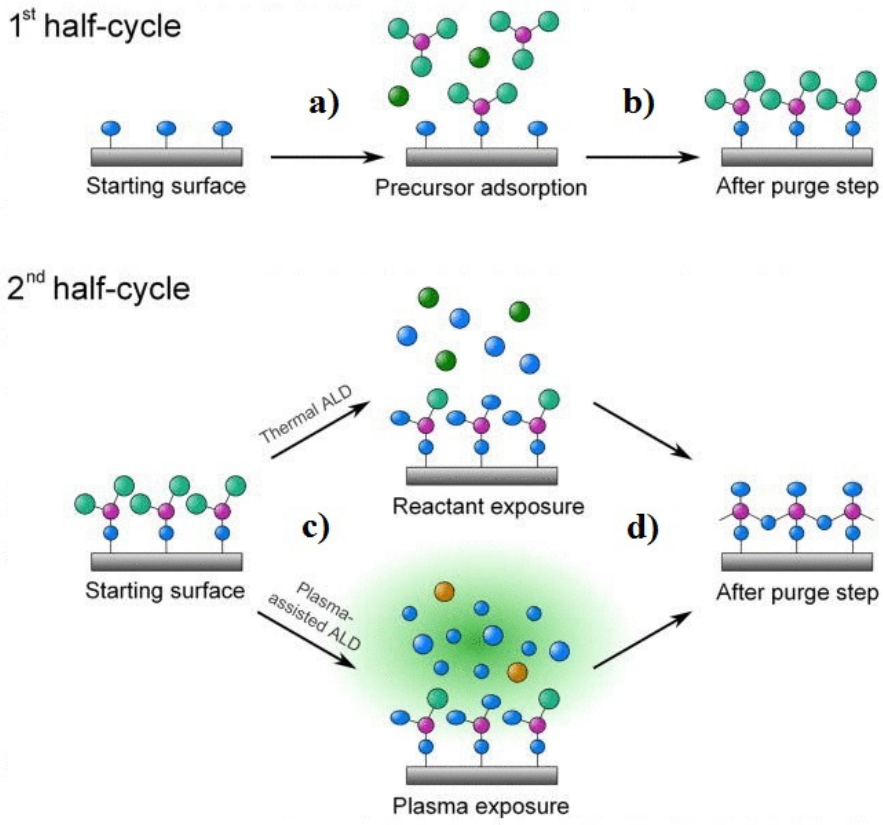

Figure 23: Four main steps of the ALD: a) Reactant is pulsed into the chamber under vacuum to react with the substrate surface. b) A first purge step. c) The second reactant is pulsed into the chamber. d) The second purge step. [56]

are pulsed on the substrate. Traditional ALD is thermally functional, it uses a sufficiently high temperature to obtain the desired chemical reaction. Although most of the ALD-materials can be deposit by using a thermal ALD but some metals, metal oxides and nitrometallic are less reactive materials and require more energy that the chemical reaction could happen. So it has been necessary to develop alternative deposition tecnique such a plasma-enhanced ALD, PEALD or plasma ALD. [52,56,57]

4.2 Plasma-enhanged ALD

Both samples of this work have been made with PEALD, therefor more details will be discussed here. Plasma is the so-called fourth state of matter. It is the practice of molecules or atoms that form a very large energetic particles containing cloud. This is achieved when the gas is heated above a certain temperature point. Plasma contains an average number of positively and negatively charged particles, and thus it is charge neutral. In PEALD a chemical reaction can happen in the ALD-chamber easily just because of these high energy particles.

PEALD has a lot of advantages compared to the thermal ALD. With plasma a chemical reaction process is more easily producible than the thermal process

and hence it offers more freedom in selecting the deposition parameters. Because radicals in the plasma and additional parameters can be adjusted, so the deposited material composition can be controlled. In addition, it gives the chance to deposit the single-element of ALD materials from metals and semiconductors that can not be manufactured by thermal ALD. PEALD has produced materials that can have better film density, the smaller impurities and better electrical properties as that produced by thermal ALD. In PEALD the substrate temperature does not need to be as high because the energy required for a chemical reaction is in a high energetic plasma particles. In addition, PEALD has a generally higher rate of growth than the thermal ALD, which is an important feature just because of using ALD technique the most restrictive factor is just very slow deposition rate compared to other techniques. Slowness is due to that the layer by layer deposition steps have to do pulsing and purge separately for all substances. [56]

4.3 Materials

It has become clear that the reactants pulsed into the ALD chamber are called precursors. First step precursor is a basic element such as a metal or a semiconductor. Second step, the precursor is a single gas such as oxygen, hydrogen or nitrogen. The precursor chemicals are usually molecules that contain material of what one wants to grow, for example, aluminum, titanium, or erbium. Plasma gases in PEALD are typically O_2, H_2, N_2, or any combination of these. Table 2 shows the materials which have been deposited with PEALD and process used the radical. [56]

One of the ALD drawbacks is that there is only a limited number of the available precursors, because most of ALD materials require effective pathways for the chemical reactions. In addition, there are some important single-element metals, such as copper, which can not be effectively grown by the available ALD methods. [58]

Table 2: Materials with PEALD. [56]

Plasma	H_2	O_2	N_2, N_2O or NH_3	H_2/N_2	O_2/N_2
Material	Ag, Al, Al_2O_3, Co, Cu, $GeSb_xTe_y$, HfN, NbN, Ni, Ta, TaC_xN_y, TaN_x, Ti, TiN_x, $TiAl_xN_y$, ZrN	Al_2O_3, $AlSi_xO_y$, Co_3O_4, $\mathbf{Er_2O_3}$, Ga_2O_3, HfO_2, $HfAl_xO_y$, $HfSi_xO_y$, La_2O_3, $LaHf_xO_y$, Pt, PtO_2, Ru, SiO_2, SnO_2, SrO, $SrTaO_6$, $SrTiO_3$, TaO_x, TiO_2, $TiSi_xN_y$, Y_2O_3, ZnO, ZrO_2, ZrN	Al_2O_3, AlN, $AlTi_xO_y$, Co, $CoSi_2$, HfN, HfO_2, Ir, NbN, Ni, $NiSi_2$, Ru, SiO_2, SiN_x, TaC_xN_y, TaN_x, TiN_x, TiO_2, $TiAl_xN_y$, WN_x, ZnO, ZrN	AlN, Co, HfN, NbN, Pd, Ru, TaN_x, TiN_x, $TiAl_xN_y$, $TiSi_xN_y$, ZrN	Al_2O_3, AlO_xN_y, $AlSi_xO_y$, HfO_2, HfO_xN_y, SiO_2, TiO_2, TiO_xN_y, ZrO_2

5 Research methods

This chapter describes the experimental methods and methodological choices for measurements.

5.1 Measurement methods

Signal attenuation is one of the most important parameters of optical waveguides. Thus, reliable measurement methods have been developed for characterization of signal attenuation. The so-called cutback method was used in this work, because it is well suited for processing of different dimensions, wavelengths, pump powers and annealing parameters changes. The used method and its alternative methods are described in the following chapter.

5.1.1 Cutback Method

The Cutback method is a simple approach for determining the propagation losses of a waveguide. Similar waveguides with different lenghts are measured with the same coupling efficiency and the input power is compared with the output powers relative to waveguides length. With this approach, the coupling losses are eliminated off and the obtained results are solely from the type of the waveguide propagation loss.

In principle, two different lengths are sufficient for calculation of the propagation losses. In practice we measure the output power P_1 of a waveguide with length L_1 and then we measure the output power P_2 of the same kind of waveguide with length L_2. In principle it is possible to calculate the losses from two waveguides with different lengths, however more reliable results are obtained by measuring several different lengths. [22] Propagation losses can be calculated using the formula

$$\alpha = \left| \frac{10 \log \frac{P_1}{P_2}}{\frac{L_1}{L_2}} \right|, \tag{27}$$

where P_1 and P_2 are the transmittance powers and L_1 and L_2 are the lengths of the longer and shorter waveguides. The unit is dB/cm. The uncertainty in this method comes from the fact that both input and output coupling should be identical during all different measurements. In addition, all the optical waveguides needs to be of the same quality and should not contain different defects that cause extra losses. This is best achieved by measurement of a long waveguide, and then cutting it shorter the same waveguide but in a different length. [59] This can be done when measuring losses of optical fibers but not with SOI waveguides. Thus, usually a set of similar waveguides with varying lengths are fabricated on a same chip for characterization of the propagation losses for SOI waveguides.

In this work samples have a sufficiently similar manufacturing technology. In addition, the most important result of the work is about grown erbium coating gain effect. The Er/Al_2O_3 coating was made very accurately around 130 nm thick by the previously described PEALD method. One used strip waveguide length series is illustrated in Figure 24. Figure 25 shows a schematic illustration of the whole used

sample of slot waveguide series. The aim was also to find out annealing effect and therefore measurements had to be made before and after the annealing treatment.

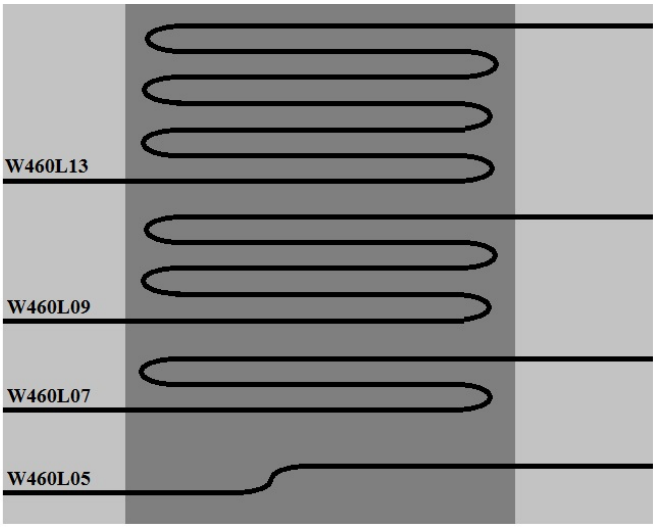

Figure 24: One of the used strip waveguides with different lengths. where W represents the waveguide width in nanometers and L the length in millimeters. The darker part of the image shows the Er/Al_2O_3 coating.

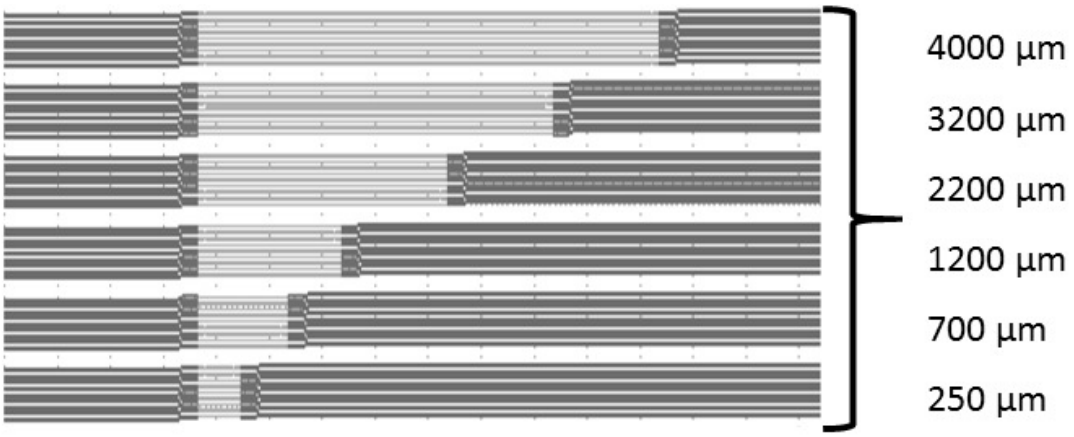

Figure 25: Schematic illustration of slot waveguides with different lengths. Each group has 9 waveguides with different slot sizes (100:20:260nm from bottom to top).

5.1.2 Sliding-Prism

Sliding-prism approach is one of the alternative methods for the evaluation of optical losses in planar waveguides. This method use a prism coupler as the sliding-prism. The prism is attached as tight as possible on slab waveguide, so that the gap between the waveguide and the prism would be very small. The contact must be really good because the evanescent field penetration depth is only about 1 μm. The laser beam

is connected to a specific input angle so that the guided mode in the waveguide appeared. A second prism coupler is attached to about 1-2cm from the input prism. Then the output power is measured using an optical power meter. The second prism is slided backward for a certain distance and the output power is measured. The propagation loss of the waveguide can be calculated when the detected power of two locations are compared. [59]

It is quite a simple operation procedure, it allows a mode-selective determination of losses and it presents also a good accuracy and efficiency. Significant disadvantages of this method are difficult to align, contact must be extremely good, surfaces have to be dirt free. [60] Also, prism coupling is only suited for coupling into slab waveguides and is thus not suitable for the strip and slot waveguides examined in this work.

5.1.3 Fabry–Perot Resonances

One possible way of measuring the waveguide propagation loss is to use it as a Fabry-Perot cavity. Waveguide's polished end facets act as mirrors creating a Fabry-Perot cavity in which the losses can be obtained from the Fabry-Perot resonances. The reflectivity of both ends is $R = (n-1)^2/(n+1)^2$ then the propagation loss α can be calculated using the formula

$$\alpha = -\frac{1}{L} \ln \left(\frac{1}{R} \frac{\sqrt{r}-1}{\sqrt{r}+1} \right), \tag{28}$$

where L is lenght of the cavity or waveguide and $r = \frac{I_{max}}{I_{min}}$ as the ratio of the maximum intensity to the minimum intensity. [61]

This method does not need knowledge of the input coupling and it is more stable, repeatable and accurate than the cutback method. But this method requires the estimation of the facet reflectivity or a technique to measure both the transmission and the reflection from the Fabry-Perot cavity, which is important especially for short waveguides. This method also needs a stabilized and narrow linewidth source, such as external cavity tunable lasers, but they are difficult to stabilize over a wide wavelength region and quite expensive. [59, 61]

5.1.4 Scattered Light Measurement

The propagation loss of a waveguide can be determined by measuring the scattered light from the surface of the waveguide. The basic principle of this method is that the amount of light scattered from the surface is proportional to the light propagating inside the waveguide. Collecting the scattered light of optical fibers can be achieved by scanning along the surface of the waveguide and then the light is collected using a lens and detected using a photodetector. An other way is by taking images of the surface using an infrared camera and the entire surfaces of waveguides are scanned by taking a series of gray images along the waveguides. The log-scale gray-level averaged power over the cross-section of a waveguide along the distance of the waveguide is then plotted and fitted using a linear equation to estimate the propagation loss of the waveguide. [62]

5.2 Coupling method

There are different techniques for light coupling. The most common ones are the end-fire, butt, prism and grating coupling methods. The basic principle of these techniques is shown schematically in Figure 26. End-fire and butt methods are used to couple beam to the end of the waveguide and coupling prism and grating coupling are coupling through the waveguide surface techniques.

Prism coupling of silicon-based waveguides is challenging, because the prism needs to be made of a material of higher refractive index than 3.5 which is the refractive index of silicon. In addition, it is practically suitable only for a planar waveguide because it can break the surface, and it must have a flat surface. Grating couplers are very suitable for coupling individual modes and for the waveguide layers of a wide range of thickness. In grating coupling technique, the input beam must be introduced at a specific angle and the angle depends on the so-called phase-matching condition. Under certain circumstances grating coupling is an effective way to couple the signal, but it requires careful design and is typically complex to manufacture, and it is not sufficiently robust for commercial devices.

End-fire and butt coupling are very similar, which are simple coupling solutions. Very important factors of these techniques are, quality of the waveguide end face, the matching of the exitation mode to the waveguide modes and the amount of reflection from the waveguide facet. There is also need to take care of the realization of the numerical aperture of the rule. [6, 7]

In this work butt coupling method with tapered polished end face fiber, as shown in Figure 27, was used. That kind of the fiber end face effectively combines the benefits of end-fire and butt coupling, as well as it helps to search the best connection point. [63]

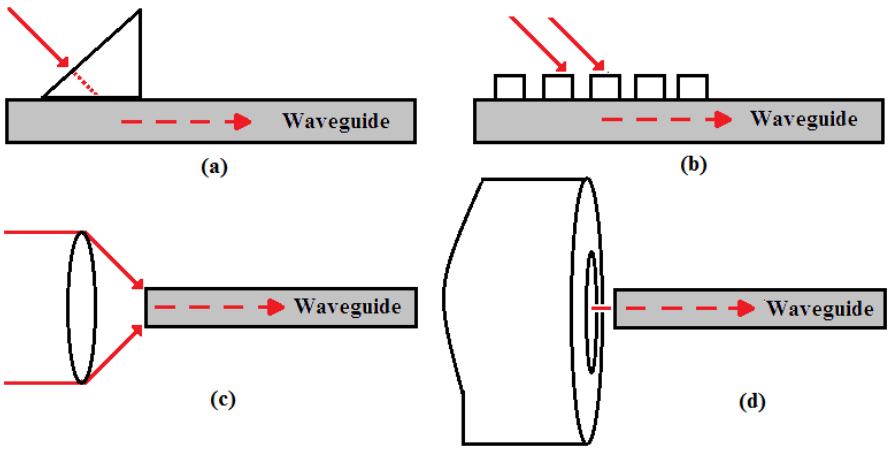

Figure 26: Four different coupling methods to the waveguide: (a) prism coupling, (b) grating coupling, (c) end-fire coupling, and (d) butt coupling.

5.3 Measurement setup and implementation method.

Figure 28 is a schematic illustration of the measurement setup which was built for the measurements conducted in this work. The following is a detailed description and the intended use of the equipment for measurements:

- Signal laser was an external cavity laser. In strip waveguide measurements, a signal of 5 mW optical power at wavelengths of 1520 nm, 1530 nm, 1535 nm, 1540 nm and 1550 nm was used. In slot waveguide measurements the same input power was used and the wavelength was scanned from 1520 nm to 1570 nm in steps of one nanometer.
- Pump laser was a narrow-band diode laser with a center wavelength of 1470 nm. The output power of the pump laser as a function of the laser diode current is shown in Figure 29.
- Red lines indicate single-mode polarization-maintaining optical fibers.
- Polarization Controllers 1 and 2 were used to adjust the output polarizations of the signal and pump lasers. Polarization controller 1 was a 3-paddle fiber polarization controller which uses the stress-induced birefringence to change the polarization and polarization controller 2 was an in-line optical fiber polarization controller which creates stress-induced birefringence within the fiber by mechanically compressing a cross-sectional axis of the fiber.
- a WDM was used to combine the signal and pump lasers into same fiber.
- Piezo controller unit (PZC) is a high-resolution nanopositioning piezo actuator unit which consists of six piezo actuators, motion controller and controller switchbox. This unit is used to control the input and output coupling fibers in the x-, y- and z-directions with nanometer-scale steps.
- Samples were two different kinds of waveguide sets which are illustrated in Figures 24 and 25. Widths of the Figure 24 strip waveguide series were 460 nm, 480 nm, 500 nm and 520 nm.
- Cam.1 and Cam.2, camera 1 together with the PZC monitored the position of the fibers ends and it was able to detect the up-conversion. Camera 2 was used for aligning the input fiber and inspecting the polarizations of both signal and pump lasers. Cam.1 is a normal CCD camera and Cam.2 is a NIR camera with a InGaAs detector.
- Polarizer for analyzing the polarization direction of the signal and pump lasers.
- Optical Spectrum Analyser (OSA) was used for collecting the spectrum and total power of the output light.
- Personal Computer (PC) was used to store data and manage the pump laser, cameras and OSA.

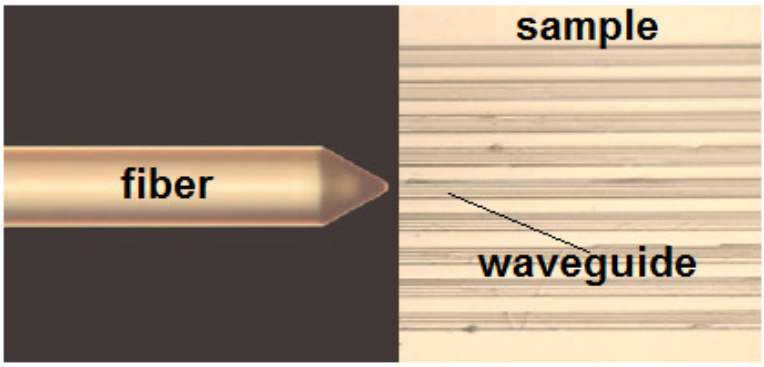

Figure 27: Butt coupling method with tapered polished end face fiber.

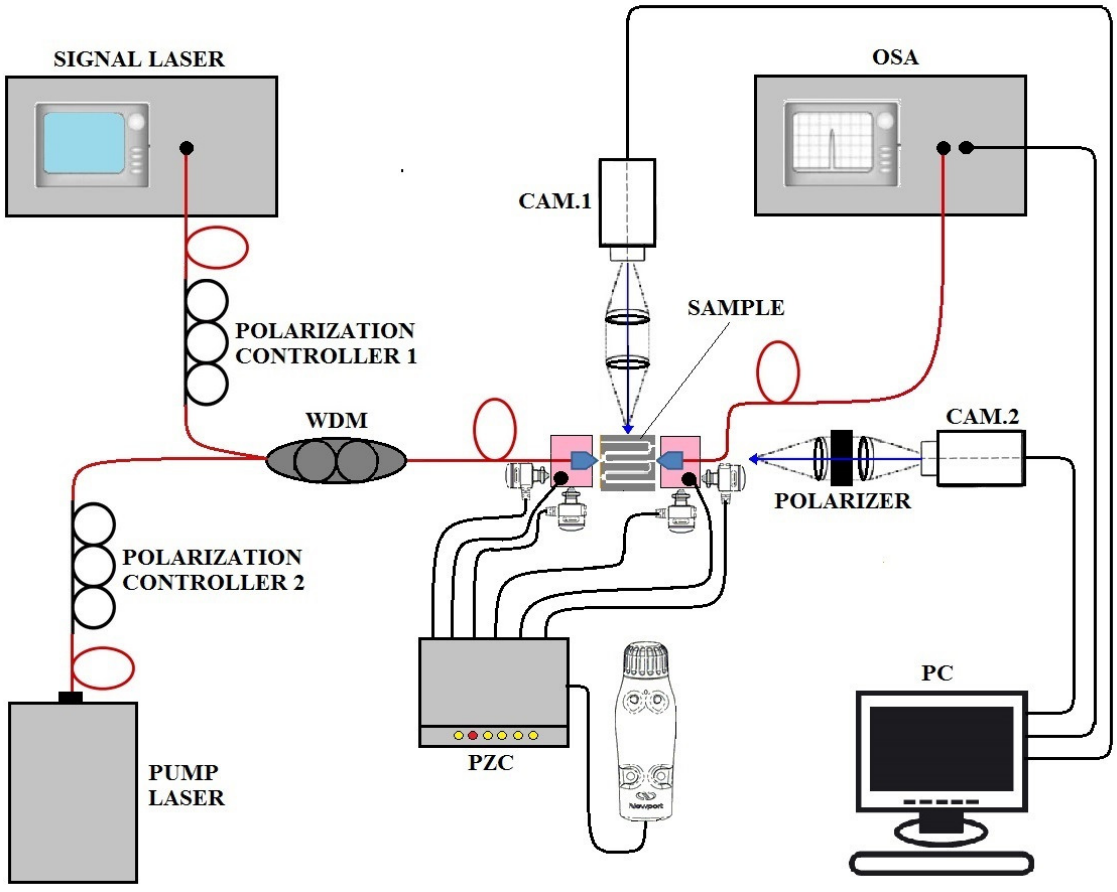

Figure 28: Schematic illustration of the measurement setup.

The work measurements were made so that each strip waveguide was measured at wavelengths of 1520 nm, 1530 nm, 1535 nm, 1540 nm and 1550 nm with transmission power 5 mW. The pump laser diode currents were set to 0 mA, 50 mA, 100 mA, 200 mA, 300 mA, 500 mA and 700 mA. Slot waveguide measurements were made by the same way except each waveguide was measured by using a wavelength scanning range from 1520 nm to 1570 nm.

Figures 30 and 31 show cross-sections of the waveguide structure of both the sample and the illustration of the light distribution into waveguides. In strip waveguides TM-mode was used and in the slot waveguides TE-mode. This was to maximize the overlap of the propagating mode with the erbium doped section of the waveguide. The input polarization was controlled by the polarization controllers 1 and 2 at the same time by observing the intensity of the light which went through the polarizer with camera 2. There was thus obtained the measurement data which could be compared to the lengths of the waveguides as well as other dimensions, wavelengths and pump powers effects in relation to each other.

In addition, the strip waveguide samples were annealed at 800°C temperature for 30 minutes and then the same measurements were made again after the heat treatment. The heat treatment was made in Micronova cleanroom under a nitrogen atmosphere. The temperature and time were optimized previously on the basis of annealing of the same types of samples [20].

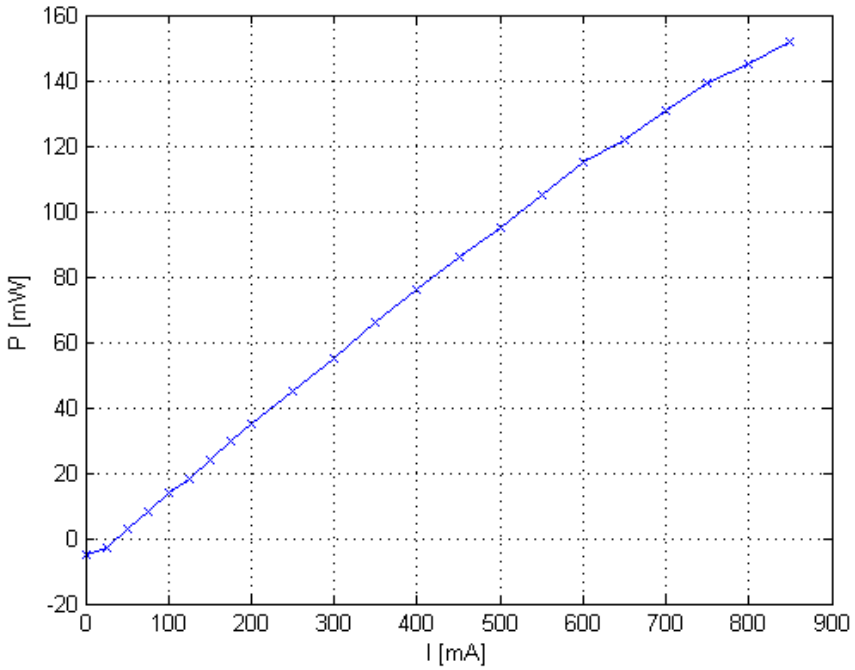

Figure 29: Measured output power P of the 1480 nm pump laser source as a function of the used current of the diode.

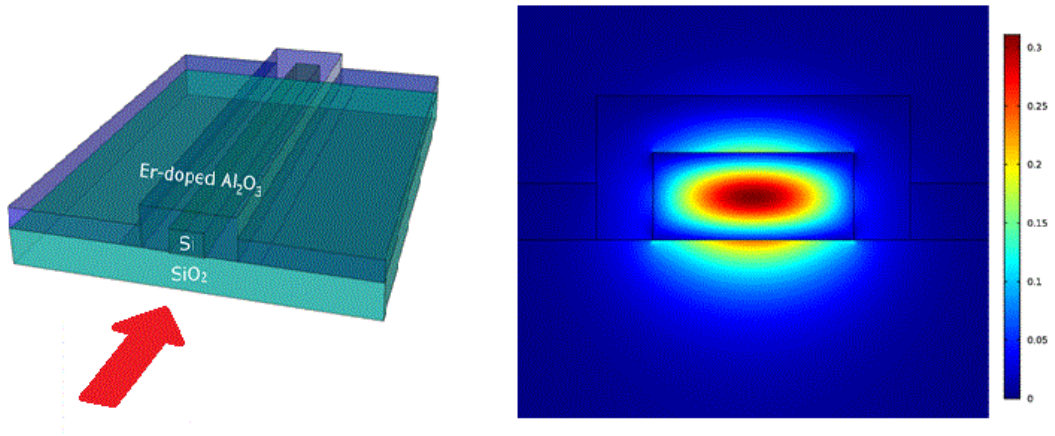

Figure 30: The cross-section of the used strip waveguide structure and the illustration of the electric field distribution in the waveguide with TM-polarization mode from [64] with permission.

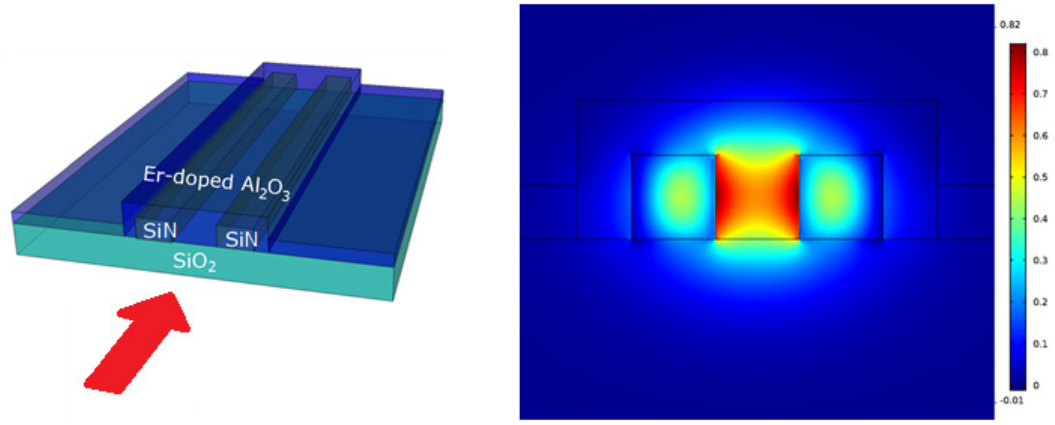

Figure 31: The cross-section of the used slot waveguide structure and the illustration of the electric field distribution in the waveguide with TE-polarization mode from [64] with permission.

6 Results

6.1 SOI strip waveguides

The measurement results of a 480 nm wide strip waveguide at different wavelengths are shown in Figures 32, 33, 34 and 35. The propagation losses without pump are shown in panel a) in each figure. Panels b), c), d) and e) illustrate signal enhancement of different length waveguides as a function of pump power. These figures show clearly that the effect of pump power is not yet saturated as the best results were obtained with the maximum available pump power. Insertion loss remained about the same for all measurements. Propagation loss is calculated by fitting Equation 29 to measured data obtained with the cut-back method. The equation that was used is

$$\gamma = \alpha \times L + \beta, \tag{29}$$

where, γ is the measured signal in dB, α is the contribution of propagation losses (dB/cm), L is the length of the waveguide and β is the contribution of insertion losses. At wavelength of 1520 nm, the propagation loss was significantly larger than that in other wavelengths, as it should be the basis of the theory [15]. The above issues were correct in principle, also in 460 nm and 500 nm wide strip waveguides. From Figure 33a it can be seen that the propagation losses are 10.97 dB/cm without pump at wavelength 1530 nm. 5.11 dB signal enhancement is achieved in 13 mm long waveguide with 135 mW pump power. Thus, contribution of propagation loss is 1.3 cm $\times$ 10.97 dB/cm = 14.26 dB, and taking into account the signal enhancement 14.26 dB - 5.11 dB = 9.15 dB, which shows that even with $\sim$ 5 dB signal enhancement, internal net gain cannot be achieved as the increased absorption caused by the erbium ions will override the enhanced signal in long waveguides.

The propagation losses, before the deposition of erbium oxide, of the strip waveguides used in this work are in the order of 5 dB/cm. This value is based on similar strip waveguides fabricated with the same method as the samples used in this work [65]. It can be approximated that from the measured 10.97 dB/cm of our Er doped silicon waveguides, we can deduce that approximately 6 dB/cm is caused by erbium. Higher quality strip waveguides are possible to fabricate, normally good quality SOI strip waveguides have propagation losses in the order of $\sim$ 1 dB/cm [38]. With optimal initial losses of 1 dB/cm, the propagation losses would be increased to 7 dB/cm after deposition of erbium. Based on the measurement results of 480 nm wide strip waveguide at the wavelength of 1530 nm and at a maximum pumping capacity, in the case of optimal quality strip waveguides it would be possible to get, 7 dB/cm $\times$ 1.3 cm - 5.11 dB = 3.99 dB, but there is still no internal net gain. With the shortest waveguide (5 mm), the situation is slightly better. The best signal enhancement was 3.03 dB and similarly with using 10.97 dB/cm propagation loss we get -10.97 dB/cm $\times$ 0.5 cm + 3.03 dB = -2.45 dB loss. With optimal 1 dB/cm and 6 dB/cm caused by the erbium this would give -0.47 dB loss, which is already quite close to net gain.

The data shown in tables 3, 4 and 5 was obtained with maximum pump power (135 mW). The results of a series of 520 nm wide waveguides has been left out

because of quality problems, as well as irrelevant results at 1520 nm wavelength has also been omitted. Tables 3, 4 and 5 clearly indicate that the closest result to the net gain is achieved with the 5 mm long waveguides. This result is also supported by up-conversion (Figure 39). It can be seen that the pump power and thus the desired effect of erbium does not reach the final end of the waveguide. Longer waveguides only caused extra propagation loss.

As a summary, average values of measured signal enhancement at different wavelengths are shown in Table 6. From these values it can be seen that on average the signal enhancement is $\sim$ 2 dB over the whole 1530 – 1550 nm wavelength range. The results shown in Tables 3–5 are summarized in Figure 36. Each of the four panels in Figure 36 shows calculated transmission for different waveguide lengths after taking the signal enhancement and propagation loss into account. Each of the data points corresponds to measured average signal enhancement. The red shaded areas show the loss caused by erbium. The top of the shaded area is the normalized transmission after propagation through the waveguide with corresponding length, assuming no erbium coating, i.e. 5 dB/cm losses as discussed above. The bottom of the red shaded area is calculated with the measured propagation losses after the erbium deposition, i.e. 10.97 dB/cm. Thus, when the data point in Figure 36 is on top of the red shaded are it means that the signal enhancement has overridden the extra loss caused by the erbium absorption. Internal net gain would have been achieved if a data point is over 0 dB. From the Figure 36, it can be seen that the increased absorption caused by the erbium deposition have not even been compensated.

The best results are from the 5 mm long waveguides, but even in the best case the extra loss is not fully compensated. The most probable reason for why the shortest waveguides provides the best results is that the pump is not able to penetrate the whole length of the waveguide. Instead the pump is large in the beginning of the waveguide, but at the end most of the pump is already absorbed and the power is not enough to excite the erbium ions. Thus, only the beginning of the waveguide is effectively taking part in the amplification, while the rest of the waveguide is only causing extra absorption. These results imply that even shorter waveguides and larger pump power would be needed for net gain.

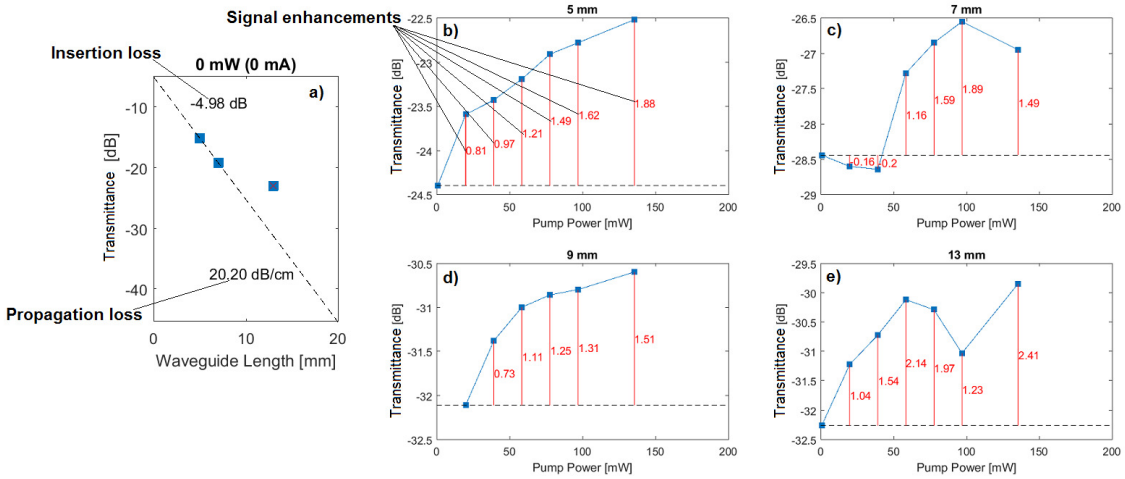

Figure 32: Measurement results of a 480 nm wide strip waveguide at the wavelength of 1520 nm. a) Insertion and propagation losses without pump. b), c), d) and e) Signal enhancement in 5, 7, 9 and 13 mm long waveguides as a function of pump power.

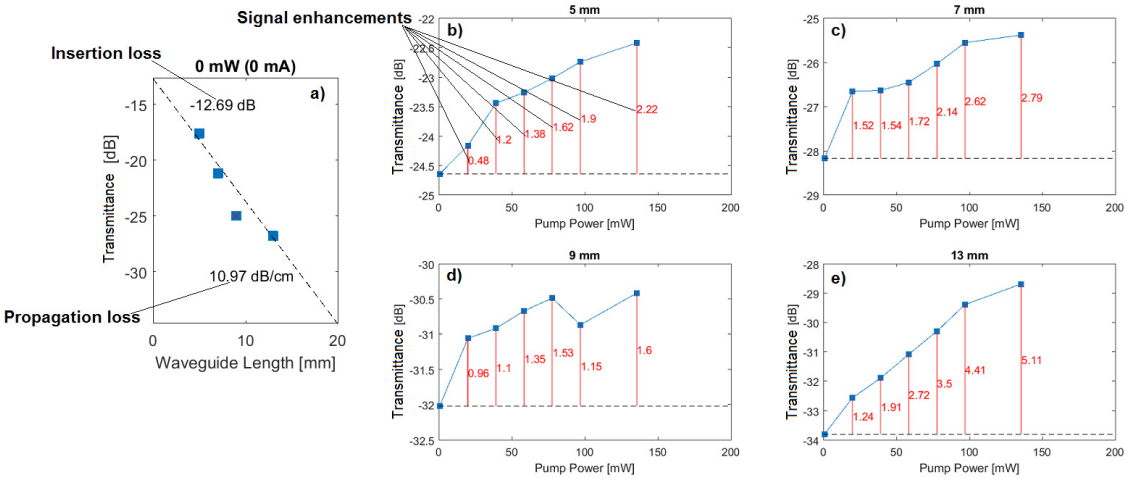

Figure 33: Measurement results of a 480 nm wide strip waveguide at the wavelength of 1530 nm. a) Insertion and propagation losses without pump. b), c), d) and e) Signal enhancement in 5, 7, 9 and 13 mm long waveguides as a function of pump power.

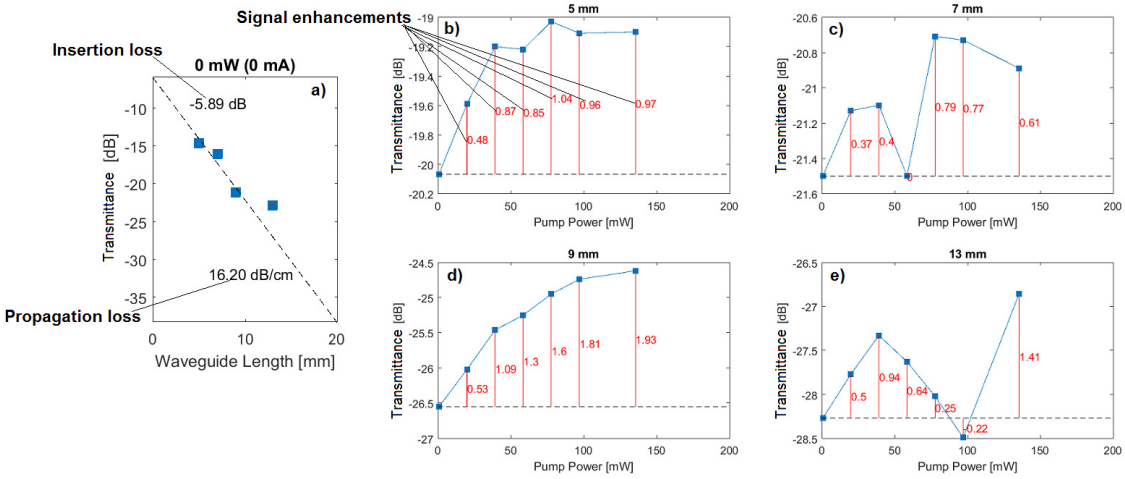

Figure 34: Measurement results of a 480 nm wide strip waveguide at the wavelength of 1540 nm. a) Insertion and propagation losses without pump. b), c), d) and e) Signal enhancement in 5, 7, 9 and 13 mm long waveguides as a function of pump power.

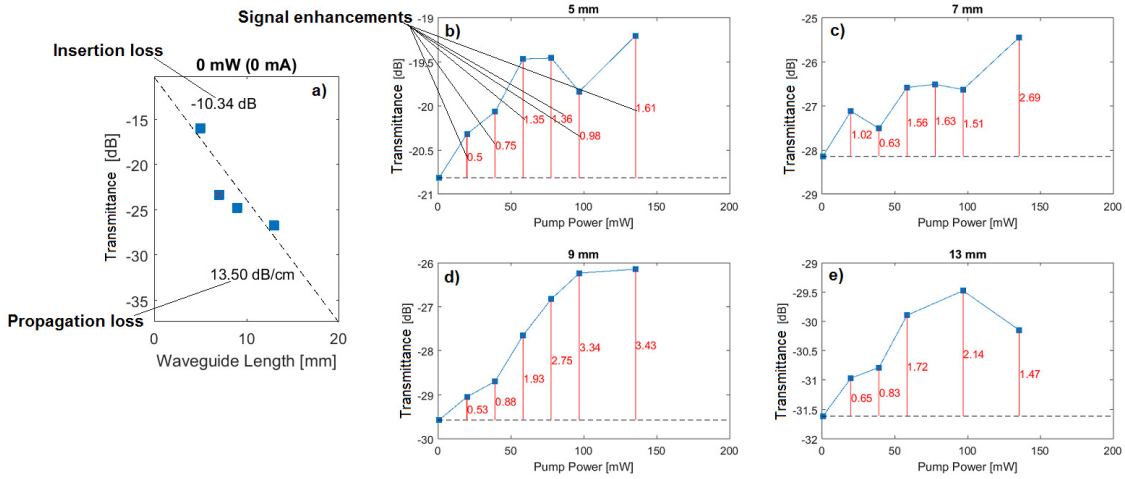

Figure 35: Measurement results of a 480 nm wide strip waveguide at the wavelength of 1550 nm. a) Insertion and propagation losses without pump. b), c), d) and e) Signal enhancement in 5, 7, 9 and 13 mm long waveguides as a function of pump power.

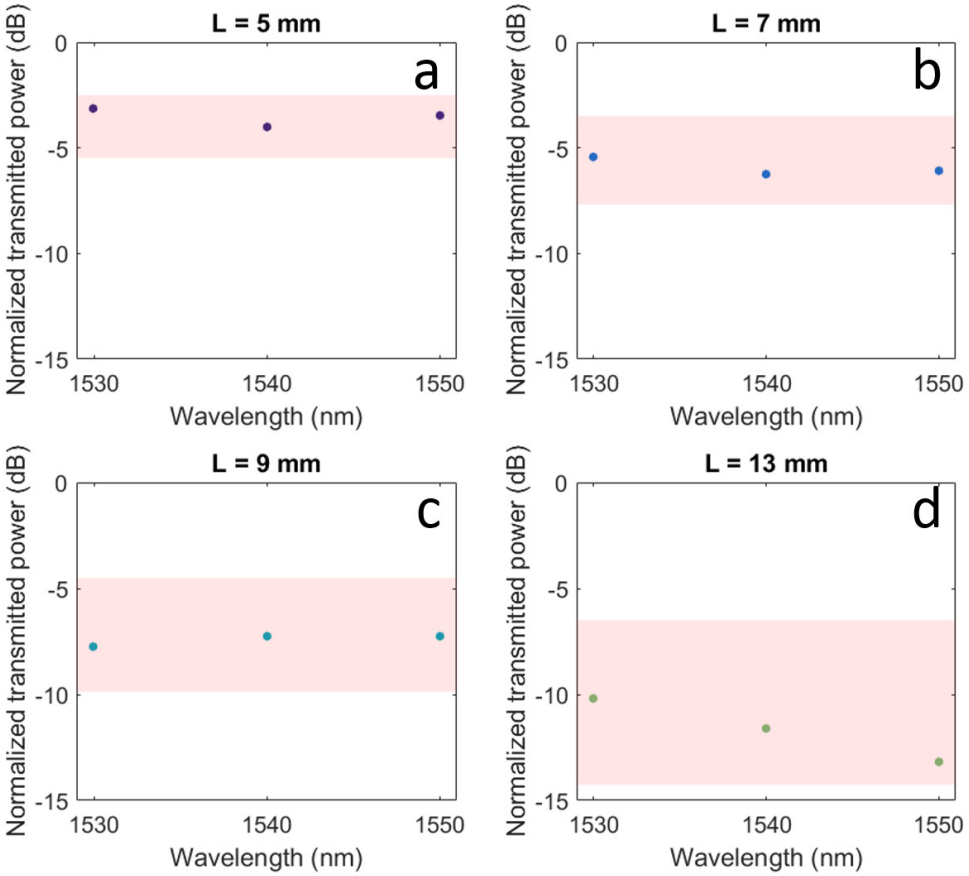

Figure 36: Signal attenuation in waveguides of different lengths, calculated using the measured average signal enhancements from several measurements and propagation losses. Waveguide lengths are a) 5 mm, b) 7 mm, c) 9 mm and d) 13 mm. The propagation losses used in the calculation were 10.97 dB/cm after the erbium deposition (bottom of the red area.) and 5 dB/cm before (top of the red area).

Table 3: Valid signal enhancement results and theoretical minimum propagation losses of a 460 nm wide strip waveguide at 135 mW pump power, at different wavelengths and at different waveguide lengths.

Wavelength [nm]	Waveguide length [mm]	Signal enhancement [dB]	Theoretical minimum loss [dB]
1530	5	1.88	1.62
1530	7	2.14	2.76
1530	9	2.68	3.62
1540	5	3.03	0.47
1540	7	1.39	3.51
1540	9	1.86	4.44
1550	5	2.39	0.74
1550	7	1.33	3.57
1550	9	2.10	4.20
1550	13	0.67	8.43

Table 4: Valid signal enhancement results and theoretical minimum losses of a 480 nm wide strip waveguide at 135 mW pump power, at different wavelengths and different waveguide lengths.

Wavelength [nm]	Waveguide length [mm]	Signal enhancement [dB]	Theoretical minimum loss [dB]
1530	5	2.22	1.28
1530	7	2.79	2.11
1530	9	1.60	3.51
1530	13	5.11	3.99
1540	5	0.97	2.53
1540	7	0.61	4.29
1540	9	1.93	4.37
1540	13	1.41	7.69
1550	5	1.61	1.89
1550	7	2.69	2.21
1550	9	3.43	2.87
1550	13	1.47	7.63

Table 5: Valid signal enhancement results and theoretically minimum propagation losses of a 500 nm wide strip waveguide at 135 mW pump power, at different wavelengths and different waveguide lengths.

Wavelength [nm]	Waveguide length [mm]	Signal enhancement [dB]	Theoretically minimum loss [dB]
1530	5	2.93	0.57
1530	7	1.90	3.00
1530	13	3.01	6.09
1535	7	2.96	1.94
1535	9	2.27	4.03
1535	13	1.42	7.68
1540	5	0.43	3.07
1540	7	2.28	2.62
1540	9	4.09	2.21
1540	13	3.89	5.21
1550	7	0.80	4.10
1550	9	2.25	4.05

Table 6: Average values of measured signal enhancements at different wavelengths.

Wavelength [nm]	Average Signal enhancement [dB]	Largest signal enhancement [dB]
1530	2.49 ± 1.70	5.11
1535	2.13 ± 0.83	2.96
1540	1.80 ± 1.52	4.09
1550	2.41 ± 1.32	4.34

6.2 SiN_x slot waveguides

Slot waveguides were analyzed in the same way as the strip waveguides. The silicon nitride slot waveguides were fabricated at the Paris-Sud University and also the propagation loss characterization was preformed there. The propagation losses were measured to be $\sim$ 4 dB/cm before the erbium deposition and $\sim$ 18 dB/cm (at 1550 nm) after the erbium deposition. It was observed that the effect of the pump power disappears even faster than in strip waveguides and that the effect of the pumping was actually well seen only in the shortest, 250 μm long, waveguides. It was also observed that the pump power is not enough to saturate the measured signal enhancement. The slot waveguides have higher losses than the strip waveguides [37, 38]. Also, the losses caused by erbium deposition were larger in the case of slot waveguides. However, because in the slot waveguides the advantage is that a larger part of the light is confined in the erbium doped layer, a relatively good signal enhancement was observed. In addition, valid results were obtained only at a wavelength of 1550 nm, which is likely due to large propagation losses and the best effectiveness of erbium at this wavelength. The measurement results of the signal enhancement of a 250 μm long slot waveguide as a function of pump power at different slot sizes W, 100 nm, 140 nm, 200 nm and 240 nm are shown in Figure 37.

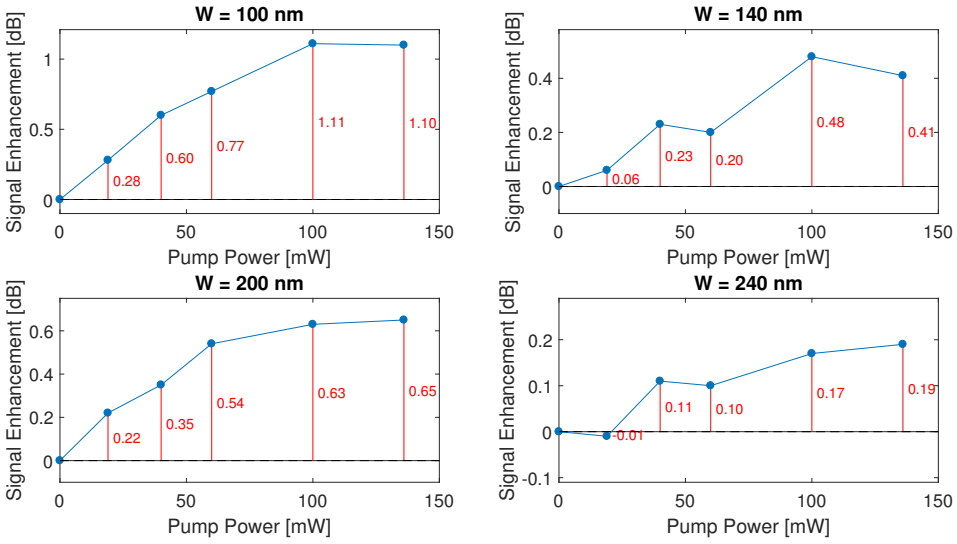

Figure 37: Valid measurement results of the signal enhancement of a 250 μm long slot waveguide as a function of pump power at different slot sizes W; 100 nm, 140 nm, 200 nm and 240 nm.

Based on the measurement results, that are shown in Figure 37, it can be seen that the maximum signal enhancement was $\sim$ 1.1 dB, with slot width of 100 nm. As in the case of strip waveguides, we calculate the signal attenuation in the slot waveguides by using the measured propagation loss and the length of the waveguide. With initial losses of 4 dB/cm the attenuation in 250 μm waveguide is 4 dB/cm$\times$0.025 cm = 0.1 dB and with 18 dB/cm it is 0.45 dB. We measured signal enhancement of

1.1 dB and thus internal net gain of $\sim$ 0.65 dB. The values in Table 7 have been calculated in this way, which shows gain values of 250 μm long slot waveguides at different slot sizes at 1550 nm signal wavelength. Maximum pump power values are used in the tables.

Similar analysis as what was performed for strip waveguides is shown in Figure 38 for the slot waveguides. However, instead of wavelength the data is shown here as a function of the waveguide length. Again the bottom edge of the red area corresponds to attenuation after the erbium deposition ($\sim$ 18 dB/cm) and the top edge to attenuation without the erbium $\sim$ 4 dB/cm. Here it can be seen that the losses are not compensated for longer waveguides but with the shortest waveguides even net gain is measured. From Figure 38 it is evident that net gain can be obtained only from short waveguides, thus limiting the possible overall amplification that is available. However, with larger pump power, more optimized coupling and further optimization of the waveguide dimensions it is possible that larger amplification can be obtained from longer waveguides.

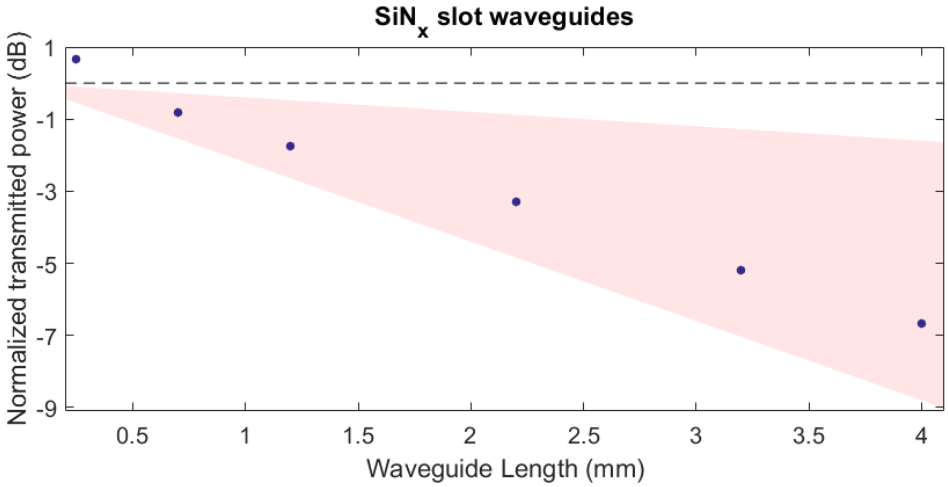

Figure 38: Signal attenuation in slot waveguides of different lengths, calculated using the measured signal enhancement and propagation losses. The propagation losses used in the calculation were 18 dB/cm after the erbium deposition (bottom of the red area.) and 4 dB/cm before (top of the red area). The horizontal dashed line displays the zero level, internal net gain is above the line.

Table 7: Calculated gain values of 250 μm long slot waveguides at different slot sizes, at 1550 nm signal wavelength and at 135 mW pump power.

Slot size [nm]	Signal enhancement [dB]	Calculated gain [dB]
100	1.10	0.65
140	0.41	-0.04
200	0.65	0.20
240	0.19	-0.26

6.3 The effects of annealing

Table 8 shows the annealing effects at different temperatures during 30 minutes of annealing. Effects are based on the previous experiments made on similar samples of atomic layer deposited Er_2O_3 films and also based on the theory of these materials [66]. Annealing was carried out at 800°C for 30 minutes.

Table 8: Effects of annealing at different temperatures. [20]

Temperature	Effect
<600°C	Hydrogen starts to move and is divided into film.
600°C-700°C	Hydrogen diffuses out of the film.
800°C	Structure of the Al_2O_3 is improved and the number of Er^{3+} ions increases.
>900°C	Erbium diffuses out of the film.

On the basis of previous study on the effect of the annealing of the erbium doped Al_2O_3 films, it was expected that the achieved amplification would be increased up to 5-10 times [20]. However, the annealing did not serve the desired purpose in this work. After the annealing, in most of the measured waveguides, the signal could not be detected any more or the observed signal was more than 10 times smaller compared to measured signal before the annealing. Reasons for the deterioration of the signal going through the waveguide could be either detachment of the waveguides from the substrate or extremely strong activation of erbium ions, which could cause significant absorption. Figure 39 shows a picture of a 500 nm wide and 9 mm long strip waveguide, before annealing, pumped with maximum available pumping capacity. It shows clearly the erbium green light emission resulting from the up-conversion. After annealing, the up-conversion is not visible even at the beginning of the waveguide, where it should be very strong if the erbium would be activated as desired. The most likely cause is partial detachment of the waveguides from the oxide layer due to thermal stress.

The sample containing slot waveguides was not annealed for this work because of the breakdown of the first sample after annealing. On the basis of the measurements obtained in this study, the sample is to be measured with higher pump power in the future. [66]

6.4 The reliability of the measurements

During the measurements it became apparent that the quality of the samples needs to be extremely good, that all results could be reliably compared. Some of the signals that had gone through were really weak, even if the connection into the waveguide was successful and clear. A closer examination of such waveguides, the camera 1 showed surface dirt or scratches that almost cut off the waveguide. The worst case of the dirt and scratches on the surfaces is shown in Figures 40 c and d. Another

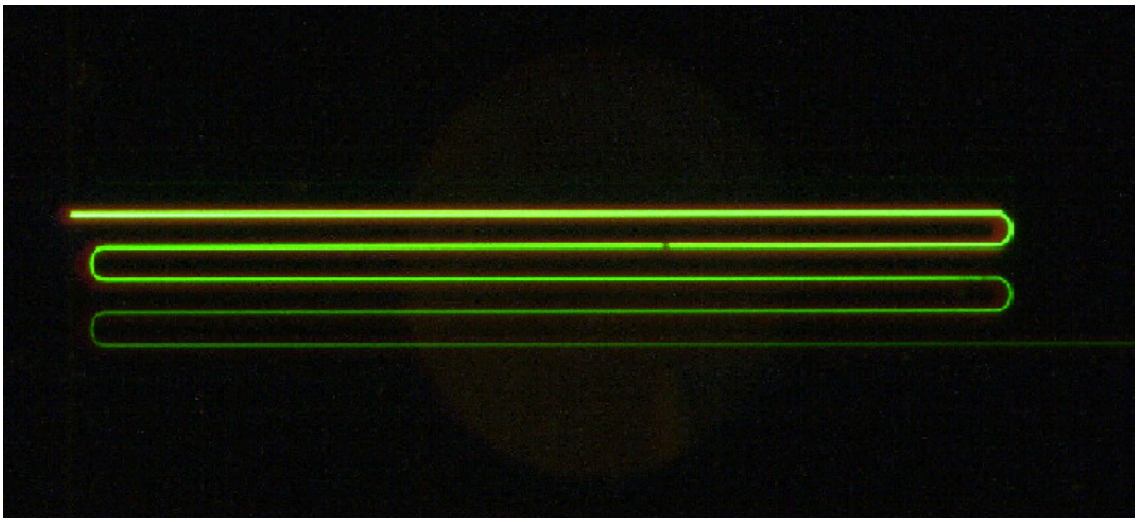

Figure 39: Up-conversion of 500 nm wide and 9 mm long strip waveguide before annealing.

important quality issue in the samples was defects at the end facets of the waveguides, examples of such waveguides are shown in Figures 40 a and b. For example, series of 520 nm wide strip waveguides have been left completely out of the results, because each waveguide was clearly of poor quality and in different condition when comparing with others.

In addition, some slot waveguides had partially unsuccessful ALD coating, due to non-conformal growth. In these cases the slots were not completely filled and an air gap could be clearly observed inside the slot. This is shown in the SEM image in Figure 41 d. Since the air gap has higher surface roughness and uneven profile along the waveguide, it causes more scattering and losses. The quality of the erbium-doped section is not comparable to completely filled slot which is shown in SEM image in Figure 41 c. The experimental data containing these identified qualitative measurement errors was omitted from the analysis. [23]

Measuring the experimental reliability and the measurement errors, the most important factor was found to be signal coupling to waveguides, which should identically good in all measurements. To make sure that the coupling efficiency was as high as possible in each measurement, several successive attempts to align the input and output fibers was made. The coupling was determined to be optimal when successive alignments produced similar output power. The coupling was found to be also very sensitive to external shocks. For example, the airflow effect of opening the door during the measurement was clearly observed in the experiments. Also long pump time most likely cause changes in the coupling efficiency due to the heating of the input fiber and the setup has to be realigned again.

Nevertheless, despite the observed uncertainties in the measurements, overall the obtained experimental data was consistent and reliable.

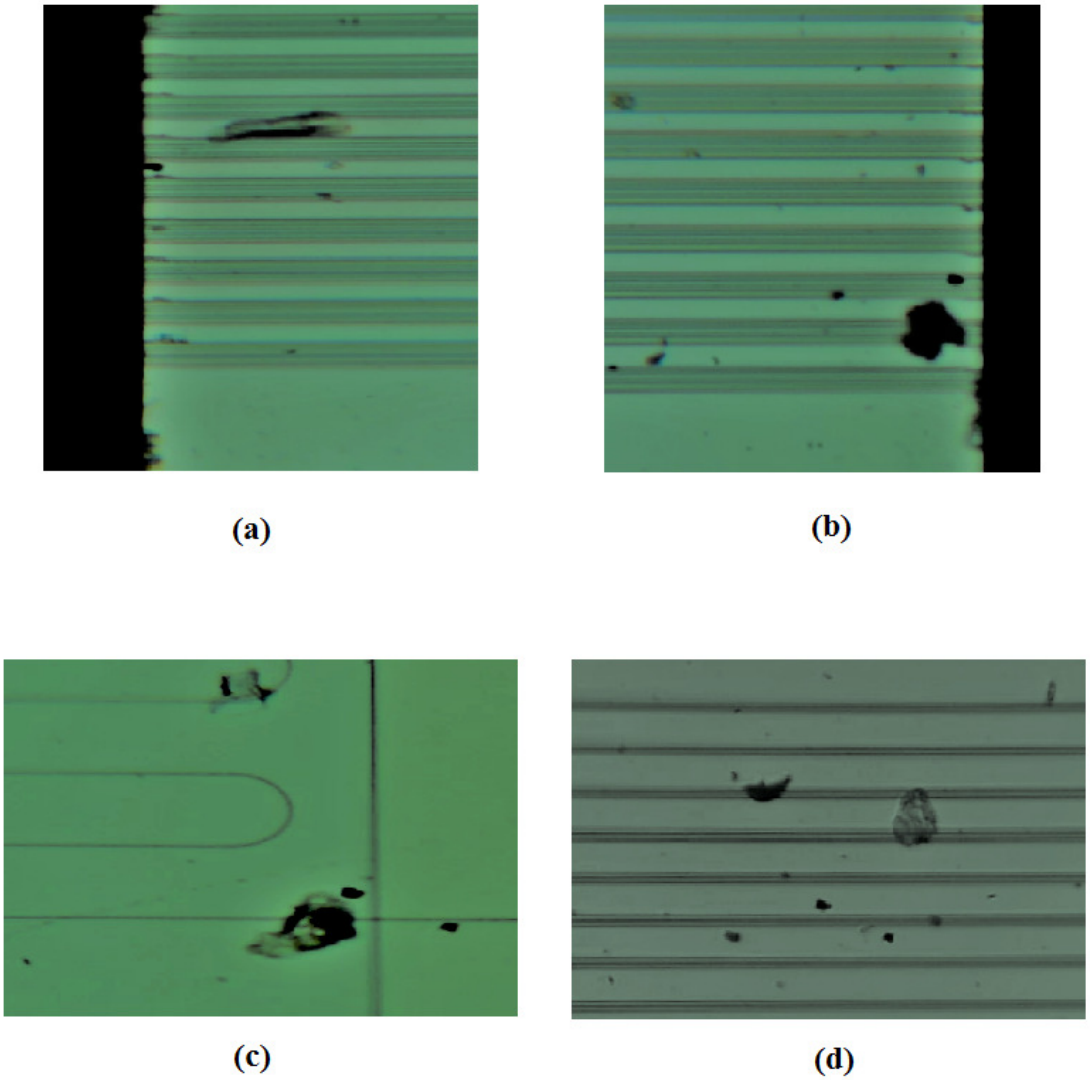

Figure 40: Surface roughness and defects in the samples.

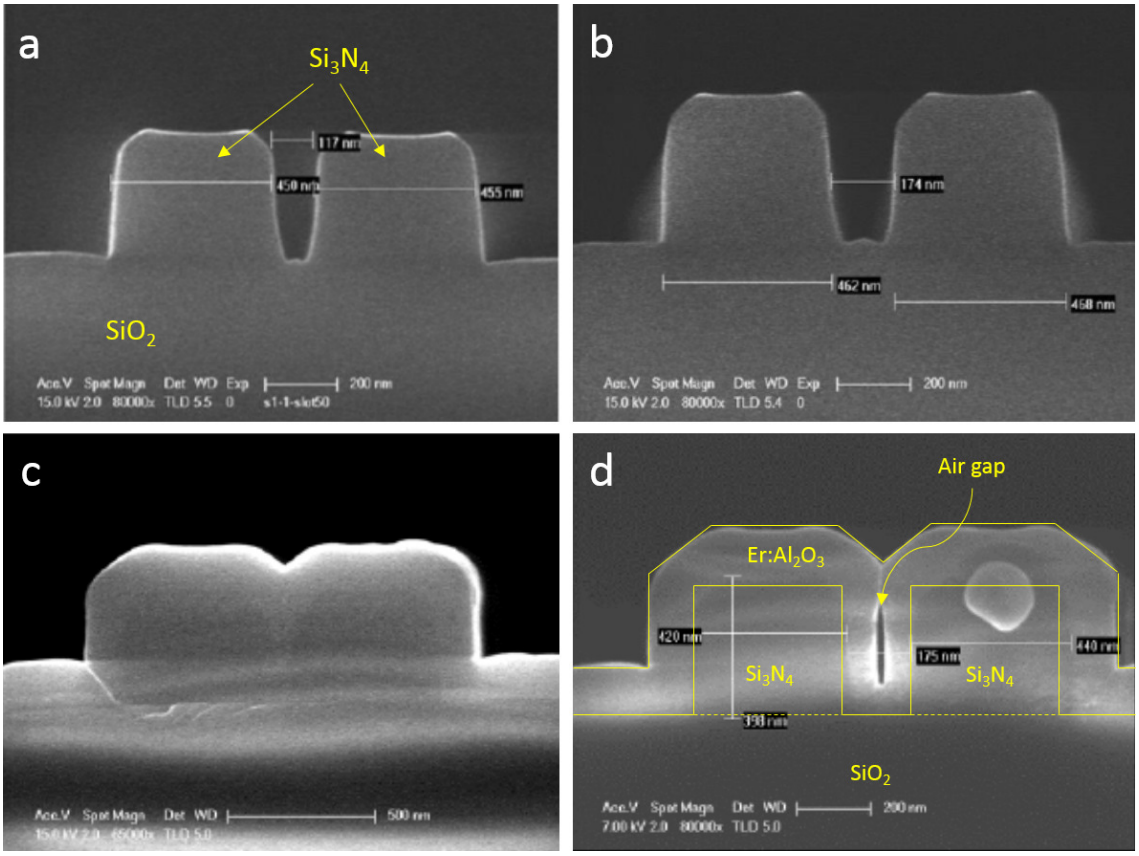

Figure 41: Scanning electron microscope images of SiN_x slot waveguides examined in this work. a) and b) waveguides with $\sim$ 120 nm and $\sim$ 180 nm slot widths before $Er:Al_2O_3$ deposition. c) and d) same waveguides as in a) and b) after the $Er:Al_2O_3$ deposition. The air gap inside the slot is clearly visible in d).

7 Conclusions

Two sets of waveguide samples (70 waveguides in total) were studied and measured in this thesis. The first set sample contained series of strip waveguides with variable dimensions and the second contained series of slot waveguides. Both samples were covered with a 130 nm thick layer of ALD grown Er-doped aluminum oxide coating. A measurement setup was built for characterizing the samples. The main aim of the study was to investigate if atomic layer deposited erbium doped coating can provide optical signal amplification in silicon based waveguides. The measurements were performed with signal wavelength ranging from 1520 nm to 1570 nm to find out the optimum wavelength for the amplification. Also the pump power was varied for investigating the most efficient pump power level for the pump at 1480 nm. Several sets of waveguides with different dimensions were tested to find the best configuration, which would bring amplification or at least bring it as close as possible to amplification.

A cut-back method was used to find out propagation losses of the waveguides. Each waveguide was measured in the wavelength range defined by the erbium emission spectrum, as well as an optical signal to be used in telecommunications with regard to important and interesting wavelength range between 1520 nm - 1570 nm. In addition, each waveguide was measured with different available pump power levels up to 135 mW at 1480 nm.

In the measurements of the samples that contain the strip waveguides, it was quickly found that with available pump power it was not possible to saturate the measured signal enhancement. The best result in almost all measurements was obtained at the maximum pump capacity. It was also clearly detectable that the propagation losses were the largest at 1520 nm wavelength, as expected from the theory. With different length waveguides, the best results were obtained for all series in 5 mm long waveguides. It can be concluded that the effect of pumping decreases with increasing length. This is due to attenuation of the pump in the longer waveguides. In longer waveguides significant portion of the pump is absorbed in the erbium-doped layer before it reaches the end of the waveguide. Thus only the beginning of the waveguide is effectively contributing to the signal enhancement. Shorter waveguides might provide better results, as was seen in the case of slot waveguides.

The best result of the strip waveguides was obtained with 5 mm long and 460 nm wide waveguides when the maximum pump power of 135 mW was used with the 1540 nm input signal. The signal enhancement was 3.03 dB and thus we get $\sim$ 2.45 dB loss, since the initial propagation losses of the waveguides used in the this study were relatively large. Assuming more optimal initial propagation losses of 1 dB/cm, this result means no more than 0.47 dB loss in the 5 mm long waveguides. This shows that internal net gain would not be possible with these samples and measurement conditions even with good quality strip waveguides. Far better results were obtained from slot waveguides. Also in the case of slot waveguides the shortest waveguides provided the best results. Internal net gain was measured at 1550 nm from 250 μm waveguides. However it must be noted that the gain was rather small which is

around 0.65 dB. The gain is limited to only the shortest waveguides. Thus, with current samples only small gain is possible to achieve with short waveguides as the attenuation increases with waveguide length. These results provide a good starting point for further optimization of both the waveguide geometry and the measurement setup.

To conclude, based on the results obtained in this work, it is evident that it is possible to achieve signal enhancement in silicon based waveguides using atomic layer deposited erbium-doped Al_2O_3 as an active material. However, the results also imply that the possible signal enhancement is limited to rather small values since the waveguide length that can be used is limited by the extra absorption caused by the erbium-doped material. With further optimization of the waveguide length, annealing process and and other dimensions of the waveguides, larger gain is possible.

During the work, I observed a lot of issues that require additional research and measurements. The biggest shortcoming of this work was the lack of a sufficiently high pump power during measurements. It would be very important to find the maximum amount of power which can still cause a signal enhancement. Measurement arrangement could also be improved by using grating coupling method. This could enhance the coupling efficiency and stability. This would be important, because a big part of the pump power was attenuated due to the low coupling efficiency. Also, the effect of air flow around the fibers should be minimized for improved stability. In- and out-coupling would be easier to make with more consistent coupling efficiency, thus providing more reliable measurements as the effect changes in the coupling efficiency would be reduced.

In conclusion, the results of this thesis clearly imply that with ALD technique, there is significant potential for realization of signal amplification in silicon based waveguides. This research definitely should be continued with the proposed improvements.

References

[1] G. Moore, "Cramming more components onto integrated circuits," *Proceedings of the IEEE*, vol. 86, pp. 82–85, Jan 1998.

[2] P. M. Becker, A. A. Olsson, and J. R. Simpson, *Erbium-doped fiber amplifiers: fundamentals and technology*. Academic press, 1999.

[3] A. Yariv and P. Yeh, *Photonics: Optical Electronics in Modern Communications*. Oxford University Press, 2007.

[4] R. Ramaswami, K. Sivarajan, and G. Sasaki, *Optical networks: a practical perspective*. Morgan Kaufmann, 2009.

[5] L. Vivien and L. Pavesi, *Handbook of silicon photonics*. Taylor & Francis, 2016.

[6] G. T. Reed and A. P. Knights, "Silicon photonics," *West Sussex, England: John Wiley and Sons, Ltd*, 2004.

[7] L. Pavesi and D. J. Lockwood, *Silicon photonics*, vol. 1. Springer Science & Business Media, 2004.

[8] C. Koos, P. Vorreau, T. Vallaitis, P. Dumon, W. Bogaerts, R. Baets, B. Esembeson, I. Biaggio, T. Michinobu, F. Diederich, W. Freude, and J. Leuthold, "All-optical high-speed signal processing with silicon–organic hybrid slot waveguides.," *Nat. Photonics*, vol. 3, no. 4, pp. 216 – 219, 2009.

[9] pveducation, Available: http://www.pveducation.org/pvcdrom/materials/optical-properties-of-silicon.

[10] B. Jalali and S. Fathpour, "Silicon photonics," *Lightwave Technology, Journal of*, vol. 24, pp. 4600–4615, Dec 2006.

[11] A. Säynätjoki, *Photonic Crystal Waveguides for Silicon Integrated Optics*. PhD thesis, Helsinki University of Technology, 2008.

[12] A. Säynätjoki, L. Karvonen, T. Alasaarela, X. Tu, T. Y. Liow, M. Hiltunen, A. Tervonen, G. Q. Lo, and S. Honkanen, "Low-loss silicon slot waveguides and couplers fabricated with optical lithography and atomic layer deposition," *Opt. Express*, vol. 19, no. 27, pp. 26275–26282, 2011.

[13] A. Kenyon, "Recent developments in rare-earth doped materials for optoelectronics," *Progress in Quantum Electronics*, vol. 26, no. 4, pp. 225–284, 2002.

[14] F. Mitschke, *Fiber Optics: Physics and Technology*. Springer Science & Business Media, 2010.

[15] J. D. Bradley and M. Pollnau, "Erbium-doped integrated waveguide amplifiers and lasers," *Laser & Photonics Reviews*, vol. 5, no. 3, pp. 368–403, 2011.

[16] G. Van den Hoven, E. Snoeks, A. Polman, C. Van Dam, J. Van Uffelen, and M. Smit, "Upconversion in er-implanted al2o3 waveguides," *Journal of Applied Physics*, vol. 79, no. 3, pp. 1258–1266, 1996.

[17] T. Alasaarela, *Atomic layer deposited titanium dioxide in optical waveguiding applications*. PhD thesis, Aalto University, 2011.

[18] E. Färm, *Selective-Area Atomic Layer Deposition*. PhD thesis, Helsingin yliopisto, 2011.

[19] S. M. George, "Atomic layer deposition: an overview," *Chemical reviews*, vol. 110, no. 1, pp. 111–131, 2009.

[20] J. Rönn, L. Karvonen, C. Kauppinen, A. P. Perros, N. Peyghambarian, H. Lipsanen, A. Säynätjoki, and Z. Sun, "Atomic layer engineering of Er-ion distribution in highly doped Er:Al_2O_3 for photoluminescence enhancement," *ACS Photonics*, vol. 3, no. 11, pp. 2040–2048, 2016.

[21] J. Rönn, "Fabrication and characterization of atomic-layer-deposited er_2o_3 for optical amplifier devices," Master's thesis, Aalto University, 2014.

[22] Y. Vlasov and S. McNab, "Losses in single-mode silicon-on-insulator strip waveguides and bends," *Optics express*, vol. 12, no. 8, pp. 1622–1631, 2004.

[23] J. Vaari, *Fysiikan laboratoriotyöt*. SFS Fysiikan Kustannus Oy, 1998.

[24] M. Bass, E. W. Van Stryland, D. R. Williams, and W. L. Wolfe, *Handbook of optics*, vol. 2. McGraw-Hill New York, 2001.

[25] M. Born and E. Wolf, *Principles of Optics*. Pergamon Press, Oxford, 1986.

[26] C. R. Pollock, *Fundamentals of Optoelectronics*. Irwin, 1995.

[27] M. Cessenat, "Mathematical methods in electromagnets," 1996.

[28] E. Hecht, "Optics 4th edition," *Addison Wesley Longman Inc, 1998*, 1998.

[29] LifeScienceSolutions, "Electromagnetic radiation," Available: http://www.olympus-lifescience.com/en/microscope-resource/primer/java/electromagnetic/.

[30] E. Ikonen, *Optiikan perusteet*. Teknillinen korkeakoulu, Mittaustekniikna laboratorio, 2001.

[31] TangientLLC, Available: https://physick.wikispaces.com /Total+Internal+Reflection.

[32] C. A. Bennett, *Principles of physical optics*. Wiley, 2008.

[33] A. Yariv, *Optical Electronics in Modern Communications*. Oxford University Press, 1997.

[34] L. Karvonen, *Nanostructures for photonic applications*. PhD thesis, Aalto University, 2013.

[35] A. Autere, "Characterization and simulation of slot waveguide devices," Master's thesis, University of Eastern Finland, 2014.

[36] the Fiber Optic Association, "Guide to fiber optics and premises cabling," Available: http://www.thefoa.org/tech/ref/OSP/fiber.html, 2010.

[37] C. C. Hu, *Modern Semiconductor Devices for Integrated Circuits*. Pearson, 2010.

[38] K. Yamada, "Silicon photonic wire waveguides: fundamentals and applications," in *Silicon Photonics II*, pp. 1–29, Springer, 2011.

[39] Refractiveindex.info, Available: https://refractiveindex.info.

[40] J. Wilson and J. F. Hawkes, "Optoelectronics-an introduction," 1989.

[41] W. T. Silfvast, *Laser fundamentals*. Cambridge University Press, 2004.

[42] O. Svelto, *Principles of lasers*. Springer, 5 ed., 2010.

[43] F. Träger, *Springer handbook of lasers and optics*. Springer Science & Business Media, 2012.

[44] M. J. Connelly, *Semiconductor optical amplifiers*. Springer Science & Business Media, 2007.

[45] D. R. Zimmerman and L. H. Spiekman, "Amplifiers for the masses: Edfa, edwa, and soa amplets for metro and access applications," *Journal of lightwave technology*, vol. 22, no. 1, p. 63, 2004.

[46] G. P. Agrawal, *Nonlinear fiber optics*. Academic press, 2007.

[47] N. N. Greenwood and A. Earnshaw, *Chemistry of the Elements*. Elsevier, 2012.

[48] P.-A. Hansen, H. Fjellvåg, T. Finstad, and O. Nilsen, "Structural and optical properties of lanthanide oxides grown by atomic layer deposition (ln= pr, nd, sm, eu, tb, dy, ho, er, tm, yb)," *Dalton Transactions*, vol. 42, no. 30, pp. 10778–10785, 2013.

[49] Igoscience, "The periodic table of the elements," Available: http://igoscience.com/periodic-table-of-elements-free-pdf/.

[50] the Royal Society of Chemistry, "Erbium," Available: http://www.rsc.org/periodic-table/element/68/erbium.

[51] P. Kik and A. Polman, "Erbium-doped optical-waveguide amplifiers on silicon," *MRS bulletin*, vol. 23, no. 04, pp. 48–54, 1998.

[52] T. Suntola, "Atomic layer epitaxy," *Materials Science Reports*, vol. 4, no. 5, pp. 261–312, 1989.

[53] M. Ventra, S. Evoy, and J. R. Heflin, *Introduction to nanoscale science and technology*. Springer Science & Business Media, 2006.

[54] J. Päiväsaari, J. Niinistö, K. Arstila, K. Kukli, M. Putkonen, and L. Niinistö, "High growth rate of erbium oxide thin films in atomic layer deposition from (cpme) 3er and water precursors," *Chemical Vapor Deposition*, vol. 11, no. 10, pp. 415–419, 2005.

[55] M. Ritala, K. Kukli, A. Rahtu, P. I. Räisänen, M. Leskelä, T. Sajavaara, and J. Keinonen, "Atomic layer deposition of oxide thin films with metal alkoxides as oxygen sources," *Science*, vol. 288, no. 5464, pp. 319–321, 2000.

[56] H. Profijt, S. Potts, M. Van de Sanden, and W. Kessels, "Plasma-assisted atomic layer deposition: Basics, opportunities, and challenges," *Journal of Vacuum Science & Technology A*, vol. 29, no. 5, 2011.

[57] M. De Keijser and C. Van Opdorp, "Atomic layer epitaxy of gallium arsenide with the use of atomic hydrogen," *Applied physics letters*, vol. 58, no. 11, pp. 1187–1189, 1991.

[58] R. W. Johnson, A. Hultqvist, and S. F. Bent, "A brief review of atomic layer deposition: from fundamentals to applications," *Materials today*, vol. 17, no. 5, pp. 236–246, 2014.

[59] X. C. Tong, "Characterization methodologies of optical waveguides," in *Advanced Materials for Integrated Optical Waveguides*, pp. 53–102, Springer, 2014.

[60] R. Ramponi, R. Osellame, and M. Marangoni, "Two straightforward methods for the measurement of optical losses in planar waveguides," *Review of scientific instruments*, vol. 73, no. 3, pp. 1117–1120, 2002.

[61] S. Taebi, M. Khorasaninejad, and S. S. Saini, "Modified fabry-perot interferometric method for waveguide loss measurement," *Applied optics*, vol. 47, no. 35, pp. 6625–6630, 2008.

[62] L. Yin, *Study of nonlinear optical effects in silicon waveguides*. PhD thesis, University of Rochester, 2009.

[63] S.-M. Yeh, S.-Y. Huang, and W.-H. Cheng, "A new scheme of conical-wedge-shaped fiber endface for coupling between high-power laser diodes and single-mode fibers," *Journal of lightwave technology*, vol. 23, no. 4, p. 1781, 2005.

[64] J. Rönn, L. Karvonen, A. Autere, A. Säynätjoki, and Z. Sun, "Atomic layer deposition of er-doped Al_2O_3 for integrated waveguide amplifier devices," *Proc. SPIE*, vol. 9750, 2016.

[65] T. Alasaarela, D. Korn, L. Alloatti, A. Säynätjoki, A. Tervonen, R. Palmer, J. Leuthold, W. Freude, and S. Honkanen, "Reduced propagation loss in silicon strip and slot waveguides coated by atomic layer deposition," *Opt. Express*, vol. 19, pp. 11529–11538, 2011.

[66] J. F. Shackelford and M. K. Muralidhara, "Introduction to materials science for engineers," 2005.